A genome-wide CRISPR/Cas9 knock-out screen identifies the DEAD box RNA helicase DDX42 as a broad antiviral inhibitor

Bonaventure Boris[1], Rebendenne Antoine[1], Garcia de Gracia Francisco[1], Tauziet Marine[1], McKellar Joe[1], Chaves Valadão Ana Luiza[1], Courgnaud Valérie[2], Bernard Eric[1], Briant Laurence[1], Gros Nathalie[3], Djilli Wassila[1], Arnaud-Arnould Mary[1], Parrinello Hugues[4], Rialle Stéphanie[4], Moncorgé Olivier[1] and Goujon Caroline[1*]

1 IRIM, CNRS, Université de Montpellier

2 IGMM, CNRS, Université de Montpellier

3 CEMIPAI, CNRS, Université de Montpellier

4 Montpellier GenomiX (MGX)

[*] Corresponding author: IRIM UMR9004, 1919 route de Mende, 34293 Montpellier cedex 5. Phone: +33 4 34 35 94 33, e-mail: caroline.goujon@irim.cnrs.fr, ORCID iD: 0000-0001-8571-1108

Genome-wide CRISPR/Cas9 knock-out genetic screens are powerful approaches to unravel new regulators of viral infections. With the aim of identifying new cellular inhibitors of HIV-1, we have developed a strategy in which we took advantage of the ability of type 1 interferon (IFN) to potently inhibit HIV-1 infection, in order to create a cellular environment hostile to viral replication. This approach led to the identification of the DEAD-box RNA helicase DDX42 as an intrinsic inhibitor of HIV-1. Depletion of endogenous DDX42 using siRNA or CRISPR/Cas9 knock-out increased HIV-1 infection, both in model cell lines and in physiological targets of HIV-1, primary CD4+ T cells and monocyte-derived macrophages (MDMs), and irrespectively of the IFN treatment. Similarly, the overexpression of a dominant-negative mutant of DDX42 positively impacted HIV-1 infection, whereas wild-type DDX42 overexpression potently inhibited HIV-1 infection. The positive impact of endogenous DDX42 depletion on HIV-1 infection was directly correlated to an increase in viral DNA accumulation. Interestingly, proximity ligation assays showed that DDX42, which can be mainly found in the nucleus but is also present in the cytoplasm, was in the close vicinity of HIV-1 Capsid during infection of primary monocyte-derived macrophages. Moreover, we show that DDX42 is also able to substantially decrease infection with other retroviruses and retrotransposition of long interspersed elements-1 (LINE-1). Finally, we reveal that DDX42 potently inhibits other pathogenic viruses, including Chikungunya virus and severe acute respiratory syndrome coronavirus 2 (SARS-CoV-2).

Over the past 20 years, a growing list of cellular proteins with various functions have been identified as capable of limiting different steps of HIV-1 life cycle (Doyle et al., 2015; Ghimire et al., 2018). Lentiviruses have generally evolved to counteract the action of these so-called restriction factors. However, type 1 interferons (IFNs) induce, through the expression of interferon-stimulated genes, an antiviral state particularly efficient at inhibiting HIV-1 when cells are pre-exposed to IFN (Ho et al., 1985; Bednarik et al., 1989; Coccia et al., 1994; Baca-Regen et al., 1994; Goujon and Malim, 2010; Cheney and McKnight, 2010). The dynamin-like GTPase MX2, and, very recently, the restriction factor TRIM5α, have both been shown to participate in this IFN-induced inhibition (Goujon et al., 2013a; Kane et al., 2013; OhAinle et al., 2018; Jimenez-Guardeño et al., 2019). With the hypothesis that additional HIV-1 inhibitors remained to be identified, we took advantage of the hostile environment induced by IFN to develop a whole-genome screen strategy in order to reveal such inhibitors.

The development of CRISPR/Cas9 as a genome editing tool in mammalian cells has been a major breakthrough, notably with the generation of pooled single guide (sg)RNA libraries delivered with lentiviral vectors (LVs), allowing high-throughput screens at the whole-genome scale (Shalem et al., 2014, 2015; Doench, 2018). We used the Genome-Scale CRISPR Knock-Out (GeCKO) sgRNA library developed by Feng Zhang's laboratory (Sanjana et al., 2014; Shalem et al., 2014, 2015) to generate cell populations knocked-out for almost every human gene in the T98G glioblastoma cell line. This model cell line is both highly permissive to lentiviral infection and potently able to suppress HIV-1 infection following IFN treatment (Supplementary Information, SI Figure 1). The screen strategy is depicted in Figure 1A. T98G cells were first modified to stably express Cas9 and a high number of T98G-Cas9 cells were then transduced with LVs coding sub-libraries A or B, the two halves of the GeCKO library. A low multiplicity of infection (MOI) was used to avoid multiple integration events and increase the probability to express only 1 sgRNA per cell. Deep sequencing analysis of the GeCKO cell populations showed more than 94% coverage for both libraries (≥ 10 reads for 61,598 and 54,609 sgRNA-coding sequences out of

65,383 and 58,029 total sgRNA-coding sequences for sub-libraries A and B, respectively). The GeCKO populations were subjected to type 1 IFN treatment in order to induce the antiviral state and, 24h later, incubated with VSV-G-pseudotyped, HIV-1 based LVs coding for an antibiotic resistance cassette. Two days later, the cells successfully infected despite the IFN treatment were selected by cell survival in the presence of the corresponding antibiotic. In order to enrich the population with mutants of interest and to limit the presence of false-positives, two additional rounds of IFN treatment, infection and selection (using different antibiotics) were performed (Figure 1A). As expected, the cells enriched after each round of the screen became less refractory to HIV-1 infection following IFN treatment (SI Figure 2).

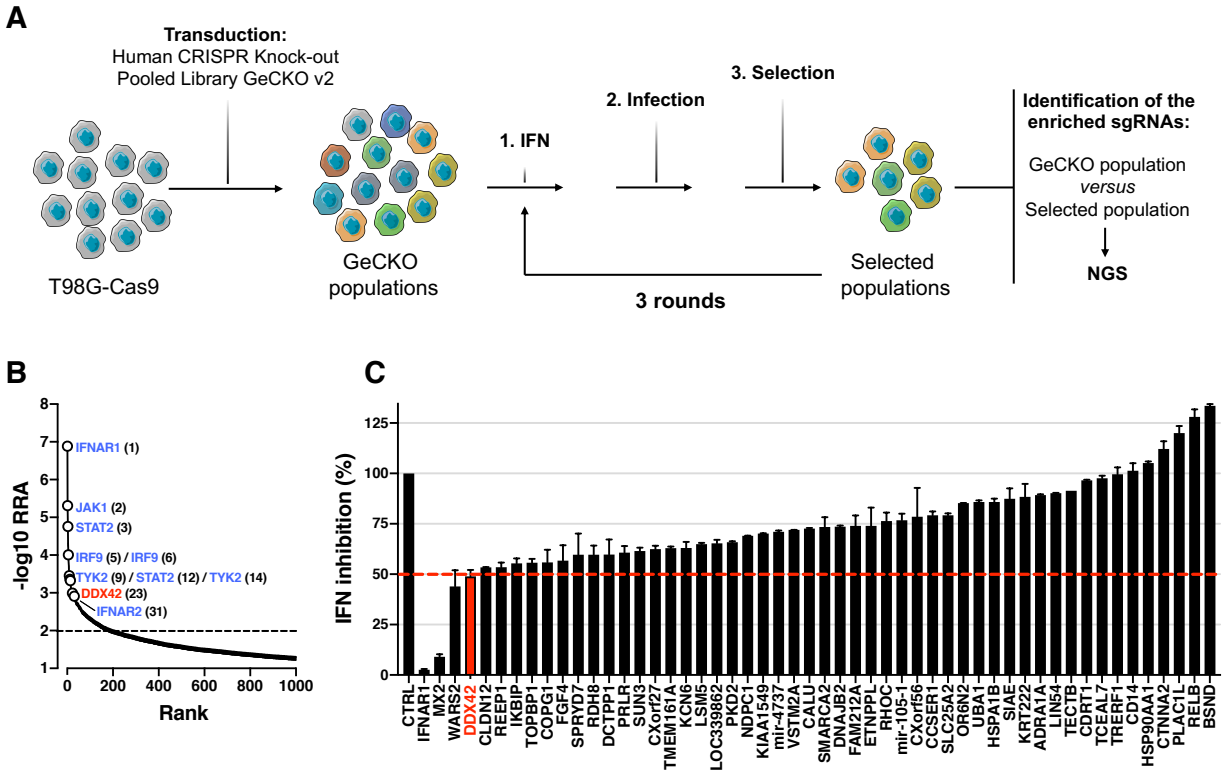

Figure 1. A whole-genome CRISPR/Cas9 screen to identify new HIV-1 inhibitors. A. Screen strategy. Model human cells (T98G) were transduced with LentiCas9-Blast LVs to generate T98G-Cas9 cells, which were then transduced with the human GeCKO v2 LV library at a MOI of 0,1 to obtain the mutant populations (GeCKO populations). The GeCKO populations were then exposed to IFN for 24h and challenged with HIV-1-based LVs coding for an antibiotic resistance gene. After selection by antibiotic addition, the surviving cells (i.e. efficiently infected despite the IFN treatment) were amplified. In total, the GeCKO population underwent three successive rounds of IFN treatment, infection and selection using LVs coding for different resistance cassettes. The genomic DNAs of the initial GeCKO populations and the three-time selected populations were extracted, the sgRNA-coding sequences were amplified by PCR and sequenced by next generation sequencing (NGS). **B**. The candidate genes were identified using the MAGeCK computational statistical tool (Li et al., 2014). MAGeCK establishes a Robust Rank Aggregation (RRA) score for each gene based on the sgRNA enrichment and the

number of sgRNAs targeting the same gene. Here, genes belonging to the IFN-response pathway (indicated in blue) and DDX42 (in red) are represented (together with their respective rank into brackets) for the 2 independent screens (the results of which were merged in the analysis). **C**. T98G/CD4/CXCR4/Cas9/Firefly KO populations were generated for the 25 best candidate genes of each screen. The control (CTRL) condition represents the mean of four negative control cell populations (i.e. expressing 4 different non-targeting sgRNAs) and IFNAR1 and MX2 KO cell populations were used as positive controls. KO cell populations were pre-treated with IFN and infected with HIV-1 Renilla. The cells were lysed 24 h post-infection and the two luciferase signals were measured (Renilla signals were normalized to internal Firefly control). The IFN inhibition (corresponding to the ratio of the untreated / IFN-treated conditions) was calculated and sets at 100% inhibition for the average of the 4 negative CTRL populations. A representative experiment is shown (mean and standard deviation from technical duplicates).

To identify the genes of interest, the differential sgRNA abundance between the starting GeCKO populations and the enriched (3-times selected) populations was analysed by NGS. 2,332 and 3,900 different sgRNAs were identified (≥ 10 reads) for screens A and B, which represented 3,6% and 7% of the sgRNAs present in the initial GeCKO population A and B, respectively. The MAGeCK algorithm, which assigns a robust ranking aggregation (RRA) score, was used to rank the gene candidates from each screen (Figure 1B). For both screens, we observed a positive enrichment for 200 genes (RRA score > 0,01), with the best hits being *IFNAR1*, *JAK1* and *STAT2* (Figure 1B). All the crucial mediators of the type 1 IFN signalling cascade were present among the top hits in both screens (with the notable exception of *STAT1*), validating our approach and confirming the identification of relevant genes. Interestingly, most of the other 195 positively selected genes displayed unknown functions or functions that were *a priori* unrelated to the IFN response pathway or to innate immunity. Of note, very little overlap was observed between the two independent screens, performed with two different sub-libraries. However, a poor overlap between independent screens has been observed before and does not preclude obtaining valid data (Doench, 2018). Therefore, the top 25 candidate genes from each independent screen were selected for further validation. As a first validation step, the sequences of the most enriched sgRNA for each gene were chosen and cloned into the LentiGuide-Puro vector (Sanjana et al., 2014). T98G-Cas9 cells expressing HIV-1 CD4 and CXCR4 receptors, as well as the firefly luciferase as internal control (T98G Cas9/CD4/CXCR4/Firefly cells), were transduced with the sgRNA-expressing LVs to generate individual KO populations. Four irrelevant, non-targeting

sgRNAs, as well as sgRNAs targeting *IFNAR1* and *MX2*, were used to generate negative and positive control populations, respectively. The KO cell populations were pre-treated with IFN and infected with an HIV-1 reporter virus expressing the Renilla luciferase reporter and bearing HIV-1 envelope (NL4-3/Nef-IRES-Renilla, hereafter called HIV-1 Renilla). Infection efficiency was analysed 30h later (Figure 1C). As expected, IFNAR1 and MX2 KO fully and partially rescued HIV-1 infection from the protective effect of IFN, respectively (Goujon et al., 2013a; Bulli et al., 2016; Xu et al., 2018). The KO of two candidate genes, namely *WARS2* and *DDX42*, allowed a partial rescue of HIV-1 infection from the IFN-induced inhibition, suggesting a potential role of these candidate genes.

DDX42 is a member of the DExD/H box family of RNA helicases with RNA chaperone activities (Uhlmann-Schiffler et al., 2006) and, as such, retained our attention. Indeed, various DEAD box helicases, such as DDX3, DDX6 and DDX17, are well-known to regulate HIV-1 life cycle (Gringhuis et al., 2017; Sithole et al., 2018, 2020; Soto-Rifo et al., 2013; Williams et al., 2015; Yedavalli et al., 2004). However, to our knowledge, the impact of DDX42 on HIV-1 replication had never been studied. In order to validate the effect of DDX42 KO on HIV-1 infection in another model cell line, two additional sgRNAs were designed (sgRNA-2 and -3) and used in parallel to the one identified in the GeCKO screen (sgDDX42-1) (Figure 2A). U87-MG/CD4/CXCR4 cells were used here, as we previously extensively characterized the IFN phenotype in these cells (Goujon et al., 2013a). Control and DDX42 KO cell populations were treated or not with IFN for 24h prior to infection with increasing amounts of HIV-1 Renilla. DDX42 depletion improved HIV-1 infection with all three sgRNAs used, confirming that endogenous DDX42 had a negative impact on HIV-1 infection. Interestingly, the increase in infection efficiency induced by DDX42 KO was observed irrespectively of the IFN treatment. DDX42 is not known to be an ISG (interferome database and our previous study (Goujon et al., 2013a), GEO accession number: GSE46599), which we confirmed in a number of cell types (SI Figure 3). The fact that the IFN-induced state is at least partially saturable (SI Figure 1) explains why an intrinsic inhibitor of HIV-1, which is not regulated by IFN, could be identified by our approach: removing one barrier to infection

presumably rendered the cells generally more permissive and, in this context, IFN had less of an impact.

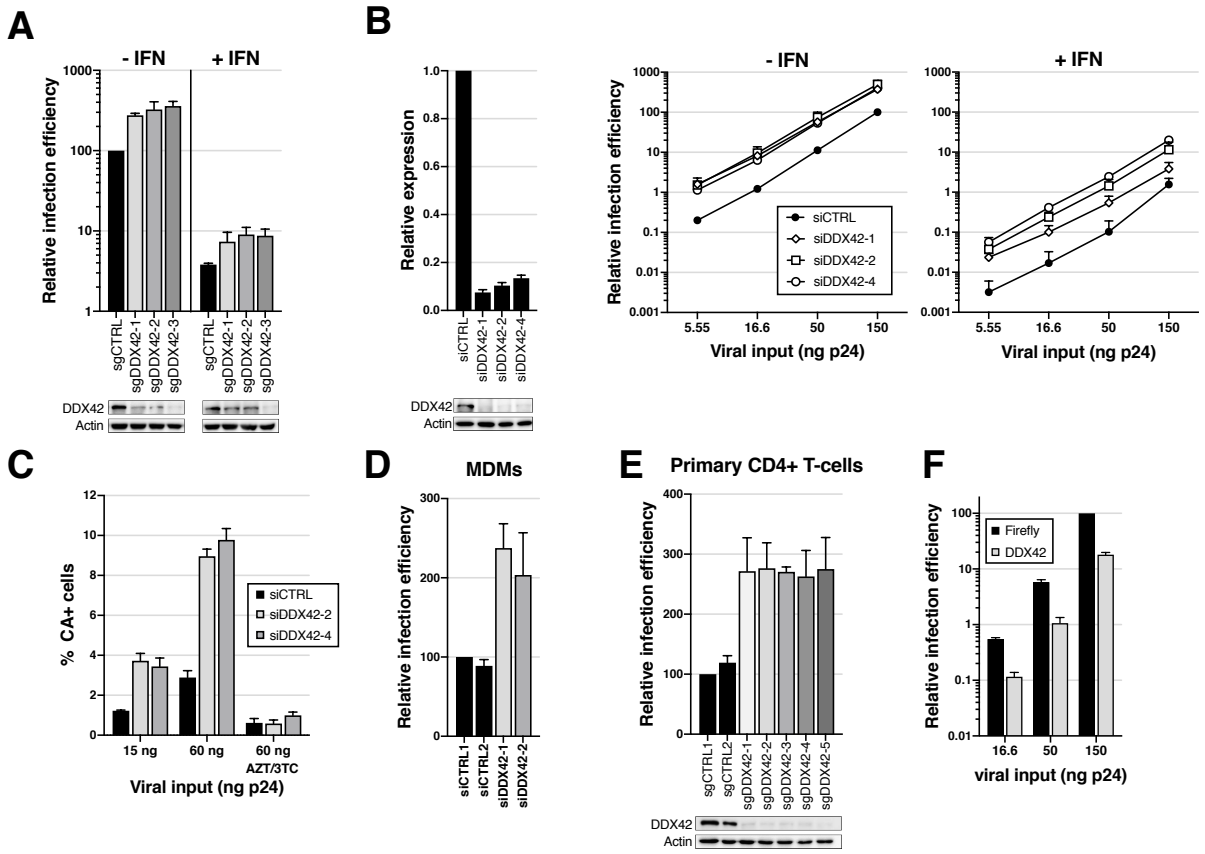

Figure 2. DDX42 is an intrinsic inhibitor of HIV-1. A. Top panel: DDX42 KO and control (CTRL) KO U87-MG/CD4/CXCR4/Cas9/Firefly cell populations were generated using three different sgRNAs (sgDDX42-1, sgDDX42-2, and sgDDX42-3) and 4 different non-targeting sgRNAs, respectively (for the CTRL condition, the average of the data obtained with the four cell populations is shown). Cells were pre-treated or not with IFN 24 h prior to infection with HIV-1 Renilla (50 ng $p24^{Gag}$) and the ratio of Renilla/firefly activity was analysed, as in Figure 1. The relative luminescence results for IFN-treated and -untreated conditions are shown. Bottom panel: Immunoblot analysis of DDX42 levels is shown for one control and the 3 DDX42-depleted populations; Actin served as a loading control. **B**. Left panel: Quantification of DDX42 silencing efficiency by RT-qPCR. Right panels: U87-MG/CD4/CXCR4 cells transfected with three different siRNAs targeting DDX42 (siDDX42-1, siDDX42-2, siDDX42-4) or a scramble siRNA (siCTRL), were pre-treated or not with IFN for 24 h prior to infection and infected with the indicated amounts of HIV-1 Renilla. The relative luminescence results for IFN-treated and -untreated conditions are shown. **C**. DDX42-depleted cells were infected with the indicated doses of HIV-1 (NL4-3) and the infection efficiency was measured by $p24^{Gag}$ intracellular staining followed by flow cytometry analysis. When indicated, the cells were treated with 10 μM zidovudine (azidothymidine, AZT) and lamivudine (3TC) reverse transcription inhibitors for 2h prior to infection. **D.** Blood monocytes from healthy donors were isolated, differentiated into MDMs, and transfected with non-targeting siRNAs (siCTRL1 and siCTRL2) or siRNAs targeting DDX42 (siDDX42-1 and siDDX42-2). Two days after transfection, MDMs were infected with a CCR5-tropic version of NL4-3-Renilla (100 ng $p24^{Gag}$). Infection efficiencies were monitored 24h later by measuring Renilla activity. The relative luminescence results from experiments performed with cells from 3 different donors

are shown. **E**. CD4+ T cells were isolated from peripheral blood mononuclear cells, activated with IL-2 and phytohemagglutinin, and electroporated with Cas9-sgRNA RNP complexes using two non-targeting sgRNAs (sgCTRL1 and sgCTRL2) and five sgRNAs targeting DDX42 (sgDDX42-1, -2, -3, -4, -5) two days later. Four days after electroporation, the activated CD4+ T cells were infected with NL4-3 Renilla for 24h. Relative infection efficiencies obtained with cells from three independent donors are shown. DDX42 protein levels were determined by immunoblot and Actin served as a loading control (a representative experiment is shown). **F**. U87-MG/CD4/CXCR4 cells stably expressing Firefly or DDX42 were infected with increasing amounts of HIV-1 Renilla. Relative infection efficiencies are shown. **A-F** Data represent the mean ± S.E.M of three independent experiments.

In order to confirm DDX42's effect on HIV-1 infection with an independent approach, we used 3 different siRNAs to knockdown DDX42 expression. We observed that depleting DDX42 with siRNAs (with >90% efficiency both at the mRNA and protein levels, Figure 2B) improved HIV-1 infection efficiency by 3 to 8-fold when using an HIV-1 Renilla reporter in U87-MG/CD4/CXCR4 cells, irrespectively of the presence of IFN (Figure 2B, right panel). Of note, wild-type HIV-1 infection was also impacted by DDX42 silencing, as shown by Capsid ($p24^{Gag}$) intracellular staining 30h post-infection (Figure 2C). We then investigated whether DDX42 had an impact in HIV-1 primary target cells. In MDMs, we observed that HIV-1 infection was increased by about 2-fold following DDX42 silencing (Figure 2D), whereas DDX42 mRNA abundance was decreased by only 40% in these cells using siRNAs (SI Figure 4). As the siRNA approach did not work in our hands in primary T cells, we used electroporation of pre-assembled Cas9-sgRNA ribonucleoprotein complexes (RNPs) to deplete DDX42 in primary CD4+ T cells (Figure 2E). Highly efficient depletion of DDX42 was obtained with all 5 sgRNAs as compared to the 2 sgCTRLs (Figure 2E, bottom panel) and this depletion increased HIV-1 infection by 2- to 3-fold, showing a role of DDX42 as an intrinsic inhibitor of HIV-1 in primary CD4+ T cells.

Having established that endogenous DDX42 had an impact on HIV-1 infection, we then analysed the consequences of DDX42 overexpression. An irrelevant control (Firefly) or DDX42 were ectopically expressed in U87-MG/CD4/CXCR4 and the cells were challenged with HIV-1 Renilla (Figure 2F). DDX42 ectopic expression induced a substantial inhibition of HIV-1 infection (about 5-fold decrease in infection efficiency in comparison to the control) (Figure 2F). We then tested a mutant version of DDX42 that is unable to hydrolyse ATP and may supposedly act as a dominant

negative, DDX42 K303E (Granneman et al., 2006; Rocak, 2005) (SI Figure 5). Interestingly, the expression of DDX42 K303E mutant increased HIV-1 infection by 3-fold, reminiscent of what we observed with DDX42 depletion. Altogether, these data showed for the first time that endogenous DDX42 is able to intrinsically inhibit HIV-1 infection.

In order to determine the step of HIV-1 life cycle affected by DDX42, we first analysed viral entry with a BlaM-Vpr assay (Cavrois et al., 2002). Consistent with the observation that VSV-G-pseudotyping did not bypass DDX42-mediated inhibition of infection (SI Figure 6), we observed that DDX42 silencing did not impact HIV-1 entry (SI Figure 7). We then quantified HIV-1 DNA accumulation over time in DDX42-silenced and control cells. DDX42 depletion increased by 2- to 5-fold the accumulation of early and late reverse transcript products (Figure 3A, B and C), as well as integrated provirus and 2-LTR circles at 48h post-infection (Figure 3D and E). More than 85% knockdown was achieved with both siRNAs targeting DDX42 (Figure 3F).

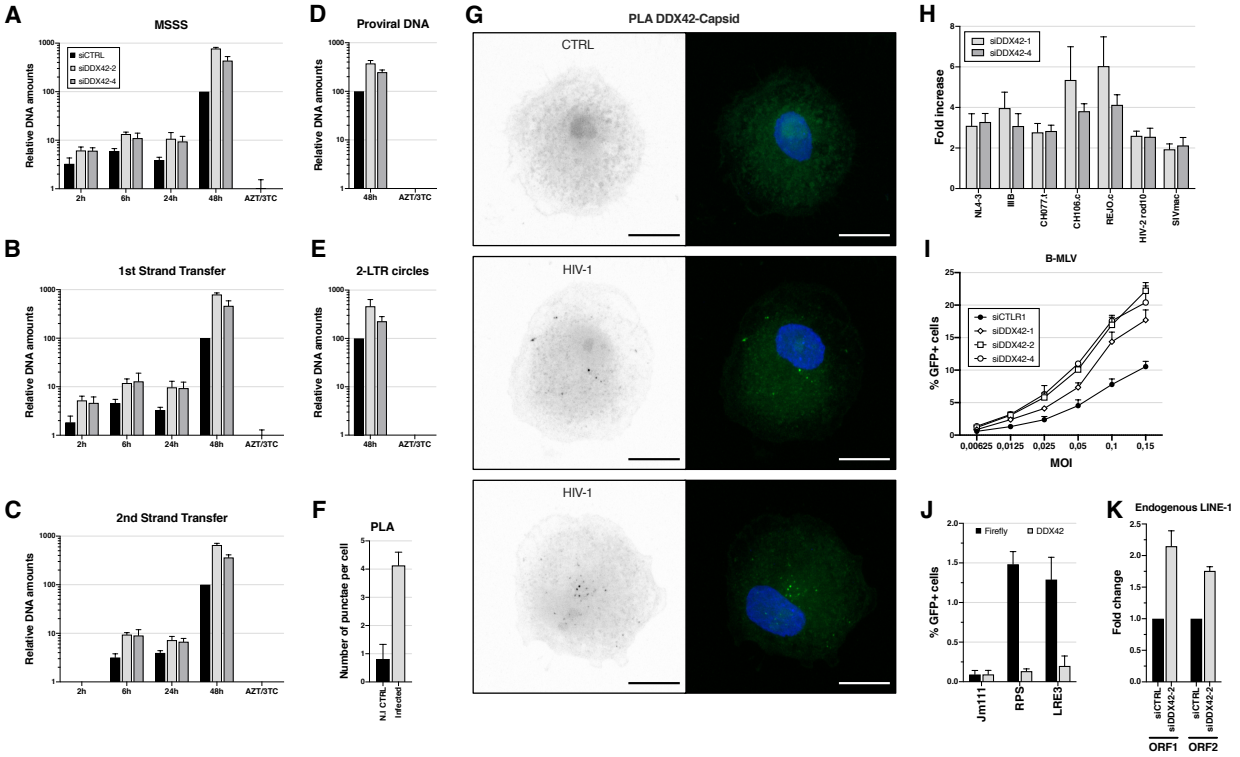

Figure 3. Endogenous DDX42 inhibits the accumulation of HIV-1 DNA, is found in close proximity to HIV-1 Capsid and inhibits retroviruses and retroelements. **A-C**. U87-MG/CD4/CXCR4 cells were transfected with a scramble siRNA (siCTRL) or DDX42-targeting siRNAs (siDDX42-2 and -4) and challenged with 60 ng $p24^{Gag}$ of HIV-1 NL4-3 72 h later. Cells were harvested at 2, 6, 24 or 48h post-infection for DNA extraction and the

relative amounts of early reverse transcript products (Minus Strand Strong Stop, MSSS, **A**, first, 1st, Strand Transfer, **B**) and late reverse-transcript products (second, 2nd, Strand transfer, **C**) were quantified by qPCR. DNA from cells infected for 48 h in the presence of 10 μM AZT and 3TC reverse transcription inhibitors was used as a control. **D-E.** The nuclear forms of HIV-1 DNA (proviral DNA**, D**, and 2-long terminal repeat (2-LTR) circles, **E**, were quantified 48h post-infection in cells previously transfected with the indicated siRNAs in the presence or not of AZT and 3TC. **F**. Proximity-ligation assays were performed in MDMs infected with HIV-1 or not (CTRL), using anti-Capsid and anti-DDX42 antibodies. Images were acquired using a LSM880 Airyscan microscope and average punctae were quantified per cell in 3 independent PLA assays done on MDMs obtained from 3 different blood donors with mean ± SEM (n>65 cells per condition, in each experiment). Statistical significance was determined by unadjusted, two-sided Mann-Whitney *U* test (****: p<0,0001). **G**. Representative images from F show PLA punctae (black, images on the left; green images on the right), nuclei stained with Hoechst (blue). Scale-bar: 10 μm. **H**. TZM-bl cells were transfected with a non-targeting siRNA or siRNAs targeting DDX42 (siDDX42-1 and -4) and infected with VSV-G-pseudotyped lentiviruses: HIV-1 NL4-3, IIIB, CH077.t, CH106.c and REJO.c, HIV-2rod10 and SIV_{MAC}. The β-galactosidase signal was measured 24 h later. The ratio of the signal in DDX42-depleted versus control cells is shown (Fold increase). **I**. U87-MG/CD4/CXCR4 cells were transfected with non-targeting siRNA (siCTRL) or siRNAs targeting DDX42 (siDDX42-1, -2, and -4) and infected and B-MLV based GFP-coding vectors, at the indicated MOIs. Infection efficiency was measured 24h later by flow cytometry. **J**. HEK293T were co-transfected with two different GFP-coding, LINE-1 plasmids (RPS-GFP and LRE3-GFP) or with an inactive LINE-1 plasmid (JM111) together with an expression plasmid coding for Firefly (as a negative control) or DDX42. GFP expression was measured by flow cytometry analysis seven days post-transfection. **K**. U87-MG cells were transfected with the indicated siRNAs and, 15 to 21 days later, endogenous LINE-1 RNAs were quantified by RT-qPCR using primers specific for ORF1 and ORF2, as indicated. Actin and GAPDH were used as endogenous controls. Fold change in ORF1 and ORF2 mRNA expression levels in DDX42-depleted cells, in comparison to the non-targeting siRNA (siCTRL)-expressing cells are represented. **A-F** and **H-K** data represent the mean ± S.E.M of three independent experiments.

These data suggested that DDX42 RNA helicase could inhibit the reverse transcription process and/or impact the stability of HIV-1 genome, leading to a decrease in viral DNA accumulation. We hypothesized that if that was the case, DDX42 should be found in close proximity to HIV-1 reverse transcription complexes during infection. In agreement with this, proximity ligation assay (PLA) performed on MDMs infected with HIV-1 showed that DDX42 could indeed be found in close vicinity of Capsid (Figure 3F and G).

We next examined the ability of DDX42 to inhibit infection by a range of primate lentiviruses including laboratory-adapted strains of HIV-1, HIV-1-transmitted founder strains, HIV-2 and simian immunodeficiency virus derived from the rhesus macaque (SIV_{MAC}). TZM-bl cells were transfected with DDX42-targeting or scramble siRNAs and infected with VSV-G-pseudotyped

lentiviruses. Infection efficiencies were monitored after 24h by measuring β-galactosidase activity (Figure 3H). DDX42 depletion increased infection levels with all the tested HIV-1 strains to the same extent than what was observed with HIV-1 NL4-3 (i.e. 3- to 5-fold). HIV-2rod10 and SIV_{MAC} infection efficiencies were also slightly improved in the absence of DDX42 (by about 2-fold). The analysis was then extended to two non-primate lentiviruses, the equine infectious anaemia virus (EIAV) and feline immunodeficiency virus (FIV), using GFP-coding LVs derived from these viruses in comparison to HIV-1 and HIV-2 LVs (SI Figure 8). DDX42 antiviral activity appeared less potent on HIV-1 LVs compared to replication-competent, full-length HIV-1, which might suggest that viral components, absent in LVs, could be playing a role in DDX42-mediated HIV-1 inhibition. Nevertheless, DDX42 depletion appeared to increase HIV-1, HIV-2 and FIV LV infection to the same extent, i.e. by about 2-fold, whereas EIAV infection was less impacted by DDX42 (SI Figure 8). We extended this study to the gammaretrovirus murine leukaemia virus (MLV) and observed that DDX42 depletion led to an increase in infection with GFP-coding MLV vectors (Figure 3I). These results strongly support a general antiviral activity of DDX42 against retroviruses.

DDX42 can be found in the cytoplasm but is predominantly located in the nucleus (SI Figure 9; Uhlmann-Schiffler et al., 2009; Zyner et al., 2019). Considering that DDX42 showed a broad activity against retroviruses and seemed to act at the level of reverse transcription, we sought to investigate whether DDX42 could inhibit retrotransposons. Long Interspersed Nuclear Elements (LINE)-1 are non-LTR retrotransposons, which have been found to be active in the germ line (Branciforte and Martin, 1994; Ergün et al., 2004; Trelogan and Martin, 1995) and in some somatic cells (Belancio et al., 2010; Muotri et al., 2005; Rangwala et al., 2009). Interestingly, DDX42 was identified among the suppressors of LINE-1 retrotransposition through a genome-wide screen in K562 cells, although not further characterized (Liu et al., 2018). To confirm that DDX42 could inhibit LINE-1 retrotransposition, HEK293T cells were co-transfected with two different, GFP-expressing LINE-1 plasmids (RPS or LRE3) or an inactive LINE-1 (JM111) together with a DDX42- or a control (Firefly)-expressing plasmid (Figure 3J). GFP-LINE-1 retrotransposition was quantified by flow-cytometry 7 days post-transfection (Moran et al., 1996). Because the GFP cassette is cloned in antisense and disrupted by an intron in this reporter system, GFP is only

expressed after LINE-1 transcription, splicing and Orf2p-mediated reverse-transcription and integration into the host genome (Moran et al., 1996). Considering that most LINE-1 replication cycles lead to truncations and defective integrations (Gilbert et al., 2005), GFP expression derived from a new integration is a relatively rare event and, as expected, the percentage of GFP+ cells observed was very low (Figure 3J). However, DDX42 ectopic expression clearly suppressed RPS and LRE3 LINE-1 retrotransposition. Indeed, while >1.25% of cells transfected with Firefly-expressing cells successfully replicated exogenous LINE-1, DDX42-expressing cells showed levels of GFP similar to what was observed with the negative control (<0.25%). To confirm that endogenous DDX42 was an intrinsic inhibitor of LINE-1 replication, we quantified endogenous LINE-1 RNA levels in DDX42-depleted in comparison to control U87-MG cells. Cells were transfected with a DDX42-targeting or a control siRNA and RT-qPCR was used to quantify LINE-1 RNA levels using 2 sets of primers and probe, specific for open reading frame (ORF) 1 and ORF2, 20 days post-transfection (Figure 3K). The depletion of DDX42 increased the levels of endogenous LINE-1 RNAs by about 2-fold, confirming a role of DDX42 in the control of LINE-1 retroelement spread.

Finally, we sought to determine whether DDX42's inhibitory activity was specific towards retroviruses and retroelements, or could be extended to other viruses. To this aim, we tested the impact of DDX42 depletion on RNA viruses from five different families: the orthomyxovirus influenza A virus (IAV), the rhabdovirus vesicular stomatitis virus (VSV), the alphavirus chikungunya virus (CHIKV), the flavivirus Zika virus (ZIKV), and the severe acute respiratory syndrome coronavirus 2 (SARS-CoV-2), responsible for the current coronavirus disease (COVID)-19 pandemic (Figure 4). Strikingly, DDX42 depletion did not have an impact on IAV or VSV replication (Figure 4A and B), thereby confirming that manipulating DDX42 expression did not have a broad and unspecific impact on target cells. However, depletion of endogenous DDX42 increased infection with ZIKV, CHIKV and SARS-CoV-2, and had a particularly high impact on the latter two (up to 1 log and 3 log increase in infection efficiency in DDX42-depleted cells in comparison to control cells, for CHIKV and SARS-CoV-2, respectively, Figure 4D and F). Of note, silencing efficiency was similar in the two types of target cells used here (Figure 4E and G).

Interestingly, DDX42 was recently identified as a potential inhibitor of SARS-CoV-2 replication in a whole-genome CRISPR/Cas9 screen in simian Vero E6 cells (Wei et al., 2020), supporting our observations that endogenous DDX42 potently inhibits the replication of this highly pathogenic coronavirus. Taken together, our data showed that DDX42 is a broad inhibitor of viral infections, albeit presenting some specificity. Further work is now warranted to explore in depth the breadth of DDX42 antiviral activity.

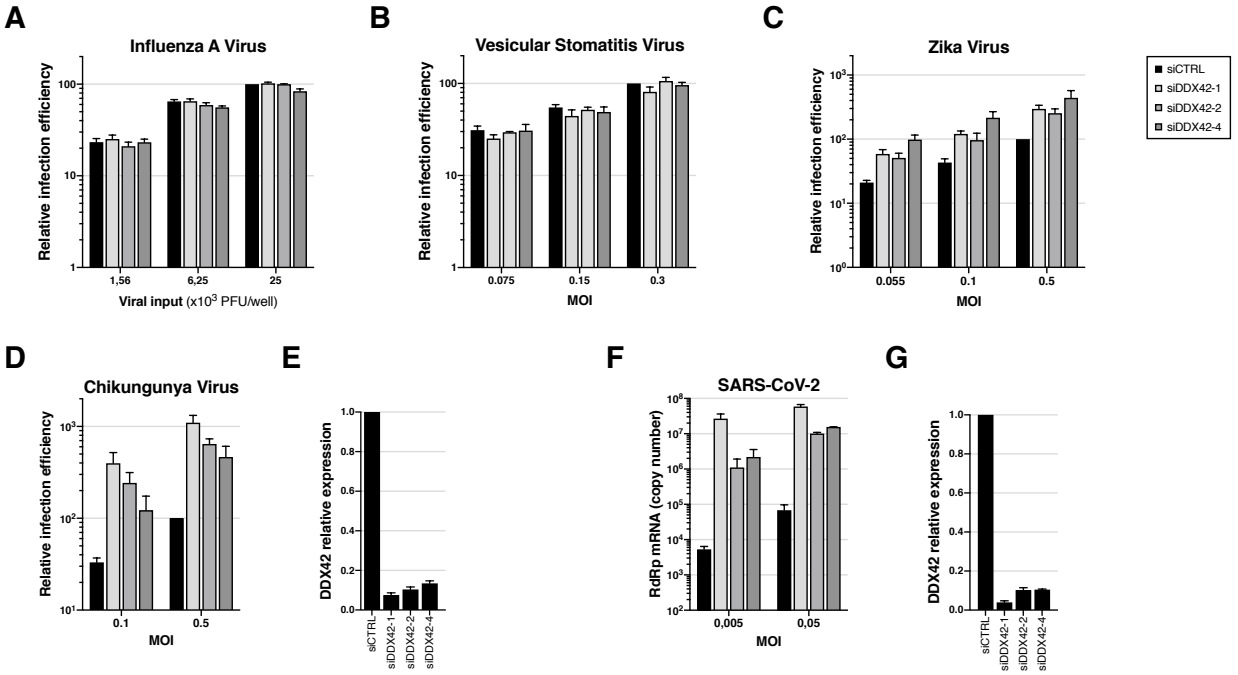

Figure 4. Endogenous DDX42 does not impact VSV or IAV infection, is a mild inhibitor of ZIKV infection and potently inhibits both CHIKV and SARS-CoV-2 replication. A. U87-MG cells were transfected with a non-targeting siRNA or siRNAs targeting DDX42 (siDDX42-1, -2 and -4) and, 72 h post-transfection, cells were infected with an influenza A reporter virus expressing Nanoluciferase. The Nanoluciferase signals were measured 16 h later. **B**. Control- and DDX42-depleted U87-MG cells were infected with a Firefly expressing VSV reporter at the indicated MOIs. The Firefly signals were measured 24 h later. **C**. Control- and DDX42-depleted U87-MG cells were infected with a Nanoluciferase-expressing ZIKV at the indicated MOIs. The Nanoluciferase signals were measured 24 h later. **D**. Control- and DDX42-depleted U87-MG cells were infected with a Gaussia-expressing CHIKV at the indicated MOIs. The Gaussia signals were measured 24 h later. **E.** Quantification of DDX42 silencing efficiency in U87-MG cells by RT-qPCR. **F**. A549-ACE2 cells were transfected with a non-targeting siRNA or siRNAs targeting DDX42 (siDDX42-1, -2 and -4). 72 h post-transfection, cells were infected with SARS-CoV-2 virus at the indicated MOIs and lysed 2 days later, their RNA contents extracted and SARS-CoV-2 replication efficiency was measured by RT-qPCR, using RdRp primers and probe. **G.** Quantification of DDX42 silencing efficiency in A549-ACE2 cells by RT-qPCR. **A-G** Data represent the mean ± S.E.M. of three independent experiments.

Here, we identified for the first time the DDX42 RNA helicase as an intrinsic inhibitor of HIV-1, capable of limiting the efficiency of viral DNA accumulation. Very few human proteins are known to inhibit this particular step of HIV-1 life cycle; these includes APOBEC3G, TRIM5α and SAMHD1 restriction factors, which are all active against HIV-1 under very specific conditions (i.e. Vif-depleted viruses, IFN pre-treatment, or in specific cell types, respectively) (Doyle et al., 2015; OhAinle et al., 2018; Jimenez-Guardeño et al., 2019). In contrast, our study revealed broad activity of endogenous DDX42 among retroviruses and retroelements, which was observed in various cell types, including primary CD4+ T cells. Interestingly, our PLA assays showed a close proximity between DDX42 and HIV-1 Capsid, which is a viral protein recently shown to remain associated with reverse transcription complexes until proviral DNA integration in the nucleus (Burdick et al., 2020; Dharan et al., 2020; Peng et al., 2014). This observation could suggest a direct mode of action on viral ribonucleoprotein (RNP) complexes. Interestingly, we observed that DDX42 was able to inhibit viruses from other families, which possess different replication strategies, including SARS-CoV-2 and CHIKV. However, DDX42 did not have an impact on all the viruses we tested, reminiscent of broad-spectrum antiviral inhibitors such as MxA, which show some specificity (Haller et al., 2015). DDX42 is known to be a non-processive helicase, which also possesses RNA annealing activities and the ability to displace RNA-binding proteins from single-stranded RNAs (Uhlmann-Schiffler et al., 2006). Moreover, DDX42 binds G-quadruplexes (Zyner et al., 2019), which are secondary structures found in cellular and viral nucleic acids and involved in various processes, such as transcription, translation and replication (Fay et al., 2017; Ruggiero and Richter, 2018). All these known activities of DDX42 would be consistent with a potential role in RNP remodeling (Uhlmann-Schiffler et al., 2006; Will et al., 2002). Nonetheless, further investigation will be needed to determine whether DDX42 acts directly by altering viral RNPs, and, if that's the case, what are the determinants for viral RNP recognition. In conclusion, this work highlights the importance of understanding the mechanism of action of DDX42 RNA helicase and its contribution to the control of RNA virus replication, an understanding which may contribute to the development of future antiviral interventional strategies.

Methods

Plasmids. The pLentiCas9-Blast, pLentiGuide-Puro vectors and the GeCKO sub-library A and B plasmids were a gift from Prof. F. Zhang (Addgene #52962, #52963, and #1000000048, respectively (Sanjana et al., 2014)). LVs coding for sgRNAs targeting the candidate genes and control genes were obtained by cloning annealed oligonucleotides in BsmBI-digested pLentiGuide-Puro, as described (Addgene). Control sgRNAs and sgRNAs targeting the candidate genes, *MX2* and *IFNAR1*, were designed with the Optimized CRISPR Design tool (not available anymore), or with Chopchop (chopchop.cbu.uib.no). The sgRNA coding sequences used were as follow: MX2 5'-CCGCCATTCGGCACAGTGCC-3', IFNAR1 5'-GACCCTAGTGCTCGTCGCCG-3', sgCTRL-1 5'-AGCACGTAATGTCCGTGGAT-3', sgCTRL-2 5'-CAATCGGCGACGTTTTAAAT-3', sgCTRL-3 5'-TTAATTTGGGTGGGCCCTGC-3', sgCTRL-4 5'-TTGGATATTAATTAGACATG-3', sgDDX42-1 5'-TCCTGAACCACACCAGCAGT-3', sgDDX42-2 5'-GGTGGTCCTGGCACTAAGCG-3', sgDDX42-3 5'-AGGCACTGTGGGACTGCTGT-3'.All the other sgRNA sequences are available upon request. In order to produce the HIV-1 based LVs used to perform the different steps of the screen (pRRL.sin.cPPT.CMV/NeomycinR.WPRE, pRRL.sin.cPPT.CMV/HygromycinR.WPRE and pRRL.sin.cPPT.CMV/ZeocinR.WPRE), neomycin, hygromycin and zeocin resistance genes (i.e. the genes coding for Neomycin phosphotransferase II, Hygromycin B phosphotransferase, and *Sh ble*) were amplified by PCR from pcDNA3.1 (ThermoFisher Scientific), pAHM (Goujon et al., 2013a), and pcDNA3.1/Zeo (ThermoFisher Scientific), respectively, and cloned by replacement of GFP in pRRL.sin.cPPT.CMV/GFP.WPRE (Goujon et al., 2008) using BamHI and SalI restriction sites. The pRRL.sin.cPPT.SFFV/E2-crimson-IRES-PuromycinR.WPRE has been described (Doyle et al., 2018). Human DDX42 cDNA was amplified by RT-PCR using the SuperScript III™ (Invitrogen) from mRNAs of MDMs and cloned by replacement of the enhanced E2-crimson in BamHI-XhoI-digested pRRL.sin.cPPT.SFFV/E2crimson-IRES-PuromycinR.WPRE, in order to obtain pRRL.sin.cPPT.SFFV/DDX42-IRES-PuromycinR.WPRE. The pRRL.sin.cPPT.SFFV/CD4-IRES-CXCR4.WPRE was obtained by replacement of E2-crimson-IRES-PuroR in pRRL.sin.cPPT.SFFV/E2-crimson-IRES-PuromycinR.WPRE with a

BamHI/SalI fragment digested CD4-IRES-CXCR4 PCR fragment obtained from pMLV-CD4-IRES-CXCR4 (a gift from Prof. N. Sherer, Wisconsin University, USA). pRRL.sin.cPPT.SFFV/Firefly-IRES-PuromycinR.WPRE was obtained by amplification of Firefly by PCR from pGL4 (Promega) and cloned into BamHI-XhoI-digested pRRL.sin.cPPT.SFFV/E2-crimson-IRES-PuromycinR.WPRE. In some experiments, LVs without a selection marker were used: the IRES-puromycinR cassette was removed by XhoI-SalI digestion and subsequent ligation, to obtain pRRL.sin.cPPT.SFFV/Firefly.WPRE and pRRL.sin.cPPT.SFFV/DDX42.WPRE. Human ACE2 coding sequence (NM_021804) was amplified using the SuperScript® III One-Step RT-PCR System with Platinum® Taq (Invitrogen) from 500 ng RNA obtained from 293T cells, using primers 5'-AATTAATTTAGCGGCCGCATGTCAAGCTCTTCCTGGCTCC-3' and 5'-AATTAATTTACTCGAGCTAAAAGGAGGTCTGAACATCATCAGTG-3, digested and inserted into NotI-XhoI-digested pRRL.sin.cPPT.SFFV/.WPRE to generate pRRL.sin.cPPT.SFFV/ACE2.WPRE (Addgene 145842). Flag-DDX42 and Flag-Firefly were amplified by PCR from the aforementioned LV plasmids and cloned into a NotI-XhoI-digested modified version of pCAGGS (Moncorge et al., 2013) to obtain pCAGGS/flag-DDX42-IRES-PuromycinR.WPRE and pCAGGS/flag-Firefly-IRES-PuromycinR.WPRE. The NL4-3/Nef–internal ribosome entry signal (IRES)-Renilla (NL4-3/Nef-IRES-Renilla) and the CCR5-version of this proviral clone were gifts from Prof. Sumit Chanda (Goujon et al., 2013b). Wild-type and Ba-L Env bearing HIV-1 NL4-3, IIIB and HIV-2 proviral clones have been described (Adachi et al., 1986; Simon et al., 1995; Schaller et al., 2011), as well as the transmitted founder HIV-1 molecular clones CH077.t, CH106.c, REJO.c (gifts from Prof. B. Hahn, (Ochsenbauer et al., 2012)) and HIV-2_{ROD10} and SIV_{MAC239} (Ryan-Graham and Peden, 1995; Gaddis et al., 2004). pBlaM-Vpr and pAdVAntage have been described (Cavrois et al., 2002). GFP-coding HIV-1 based LV system (i.e. p8.91 HIV-1 Gag-Pol, pMD.G, and GFP-coding minigenome), and HIV-2, FIV, and EIAV-derived, GFP coding LVs, as well as MLV-derived, GFP coding retroviral vectors have all been described (Naldini et al., 1996; Bainbridge et al., 2001), (O'Rourke et al., 2002; Saenz et al., 2005). The LINE-1 plasmid 99 RPS-GFP PUR (pRPS-GFP), 99 RPS-GFP JM111 PUR (pJM111) and pLRE3-GFP were developed by Prof. Kazazian's lab (Moran et al., 1996; Ostertag et al., 2000; Goodier et al., 2012).

Cell lines. Human cell lines HEK293T, A549, U87-MG, TZM-bl were obtained from the ATCC and the AIDS reagent program, respectively, and T98G cells were a gift from Prof. G. Kochs (Freiburg University, Germany). These cell lines were cultured in Dulbecco's Modified Eagle Medium (DMEM) supplemented with 10% fetal bovine serum and 1 % penicillin-streptomycin (Thermofisher). T98G-Cas9 and U87-MG-Cas9 were obtained by transduction of T98G and U87-MG, respectively, with HIV-1-based LVs expressing the spCas9-P2A-Blasticidin cassette (pLentiCas9-Blast (Sanjana et al., 2014)). U87-MG/CD4/CXCR4 have been described (Goujon et al., 2013a) and were further modified to express Cas9 and Firefly using pLentiCas9-Blast and pRRL.sin.cPPT.SFFV/Firefly.WPRE, respectively. T98G-Cas9/CD4/CXCR4/Firefly were obtained by successive transductions of T98G-Cas9 with pRRL.sin.cPPT.SFFV/CD4-IRES-CXCR4.WPRE at a high MOI, and pRRL.sin.cPPT.SFFV/Firefly.WPRE, at a low MOI, respectively. Cell surface staining with anti-CD4 and CXCR4 antibodies (Miltenyi Biotec) confirmed than more than 95% cells were positive for both markers. A549 cells stably expressing ACE2 were generated by transduction with RRL.sin.cPPT.SFFV.ACE2.WPRE containing-vector. For antibiotic selection, cells were treated with 10 μg/mL Blasticidin (InvivoGen), 1 mg/mL Zeocin (InvivoGen), 2 μg/mL Puromycin (Sigma-Aldrich), 250 μg/mL Hygromycin (Sigma-Aldrich), 1 mg/mL G418 (Sigma-Aldrich). When indicated, IFN (universal type 1 IFN, PBL Interferon Source) was added at 1000 U/mL for 16-24h prior to virus infection or RNA extraction, and AZT and 3TC (AIDS reagent program) at 10 μM for 2 h prior to infection.

Primary cells. Blood from healthy donors was obtained from the Etablissement Français du Sang, under agreement n°21PLER2019-0106. Peripheral blood mononuclear cells (PBMCs) were isolated by centrifugation through a Ficoll® Paque Plus cushion (Sigma-Aldrich). Primary human CD4+ T cells and monocytes were purified by positive selection using CD3 and CD14 MicroBeads, respectively (Miltenyi Biotec), as previously described (Goujon et al., 2013a). Monocytes were incubated for 3 hours in serum-free Roswell Park Memorial Institute (RPMI) 1640 medium and further differentiated into macrophages by culture for 5-7 days in RPMI 1640

supplemented with 10% fetal calf serum, 1% penicillin-streptomycin and 100 ng/ml granulocyte-macrophage colony-stimulating factor (GM-CSF; Miltenyi). CD4+ T cells were in cultures in RPMI supplemented with 10% fetal bovine serum and 1% penicillin-streptomycin and stimulated 48h with 10 µg/ml phytohemagglutinin (PHA) (Fisher Scientific) and 50 U/mL interleukin-2 (IL-2, Miltney Biotec) prior to electroporation.

Genome-scale CRISPR/Cas9 screens. The plasmids coding the GeCKO sub-libraries A and B were amplified and prepared according to the provided guidelines (Lentiviral Crispr Toolbox, Addgene). 60 million T98G Cas9 cells were transduced with GeCKO LVs at a MOI of 0,1 to cover about 100-times the half-library complexity. After 48h, the cells were selected with puromycin, amplified for 12-15 days. 45 million cells were harvested and frozen down at -80°C for subsequent genomic DNA extraction, using the QIAamp DNA Blood Maxi Kit according to manufacturer's instructions (Qiagen). In parallel, 60 million cells from the initial GeCKO populations were used for the screen. The cells were treated with 1000 U/mL IFN for 24h, infected with LVs coding a hygromycin resistance cassette. 48h later the cells selected with hygromycin and the surviving cells amplified. Two other rounds of IFN treatment, LV infection and antibiotic selection were subsequently performed with LVs coding a neomycin resistance cassette and a zeocin resistance cassette, respectively. The three time-selected populations were amplified and 45 million cells were harvested and stored at -80°C for subsequent genomic DNA extraction, as previously. After genomic DNA extraction, the sgRNA coding sequences integrated in the genomic DNA from the initial and 3-times selected populations were amplified by touch-down PCR and sequenced by Illumina deep sequencing. To this aim, 120 µg of genomic DNA was amplified using DNA Herculase II Fusion DNA polymerase (Agilent) in the presence of 2% DMSO, 1 mM of dNTPs; and 400 nM of the following primers: Forward-primer1: 5'-TCGTCGGCAGCGTCAGATGTGTATAAGAGACAGCTTGTGGAAAGGACGAAACACC-3' for screen A or Forward_primer2: 5'-TCGTCGGCAGCGTCAGATGTGTATAAGAGACAGGATCTTGTGGAAAGGACGAAACACC-3' used for screen B, together with reverse primer: 5'-

GTCTCGTGGGCTCGGAGATGTGTATAAGAGACAAAGGTCCATTAGCTGCAAAGATTCCTCT C-3'). Briefly, after 5 minutes at 95°C, 14 cycles of pre-amplification were performed with a hybridization temperature decreasing by 0.5°C per cycle (30 sec at 95°C, 30 sec at 60°C, 30 sec at 72°C), followed by 30 cycles of amplification (30 sec at 95°C, 30 sec at 53°C, 30 sec at 72°C). 50 ng of each amplicon was dual indexed in a 5-cycle PCR reaction using the PCR module and indexed primers from the Nextera kit (Illumina). Resulting libraries were purified on AMPure XP magnetic beads (Beckman Coulter) using a 0,8X ratio and verified on Fragment Analyzer using the HS NGS fragment kit (Agilent). Libraries were quantified using microfluorimetry (QuBit, Invitrogen), mixed with a PhiX library (Illumina) and sequenced on one single read 50nt lane of Hiseq2500 using the rapid mode.

Image analyses and base calling were performed using the Illumina HiSeq Control Software and Real-Time Analysis component (v1.18.66.3). Demultiplexing was performed using Illumina's conversion software (bcl2fastq 2.20). The quality of the raw data was assessed using FastQC (v0.11.5) from the Babraham Institute and the Illumina software SAV (Sequencing Analysis Viewer). Potential contaminants were investigated with the FastQ Screen (Wingett and Andrews, 2018) (v0.11.4) software from the Babraham Institute.

Sequencing reads were trimmed using Cutadapt (Martin, 2011) (v1.13), with options -g [primer sequence] -u [length of remaining 3' bases] -e 0.2 -m 18 -l 20, to remove primer sequences and retrieve the 20 bases long sequences corresponding to sgRNAs. These retrieved sequences were then aligned to the GecKOv2 Human Library (A or B) reference sequences (keeping only non-duplicated sgRNA sequences, the duplicated ones being annotated) using Bowtie (Langmead et al., 2009) (v1.2), with options -v 2 -norc -S. Resulting bam files were sorted and indexed using Samtools (Li et al., 2009) (v1.5). Quantification of sgRNAs was done using Samtools idxstats. MAGeCK (Li et al., 2014) (v0.5.7) was used to normalize (total count method) and identify enriched sgRNAs and genes in 3-times selected cell populations versus starting GeCKO transduced cells (mageck test command).

Lentiviral and retroviral production. To produce lentiviral vector particles, HEK293T cells were transfected by polyethylenimine (PEI) co-transfection with miniviral, HIV-1 based genome coding

plasmids (e.g. LentiCas9-Blast, LentiGuide-Puro or pRRL-SFFV), p8.91 (HIV-1 GagPol) and pMD.G (VSV-G) at a ratio of 1:1:0.5, respectively. The medium was replaced after 6h and viral particles were harvested 42h later, filtered, and directly used to transduce target cells (or stored at -80°C). After 4 to 6 hours, the transduction medium was replaced with complete DMEM, and the cells were treated 48h later with the relevant antibiotics. The HIV-2-, FIV-, EIAV-GFP coding LVs were produced using GFP-coding HIV-2-, FIV-, EIAV-based miniviral genomes, together with HIV-2-, FIV-, EIAV- GagPol, expression constructs and pMD.G at a ratio of 1:1:0.5. MIGR1 MLV-derived retroviral vectors were obtained with B-MLV Gag-Pol-expressing plasmid pCIG3B, the GFP-expressing minigenome pMIGR1 and pMD.G. at a ratio of 1:1:0.5, respectively and harvested as previously described.

HIV-1 Renilla and NL4-3 HIV-1 were produced by standard PEI transfection of HEK293T. When indicated, pMD.G was cotransfected with the provirus at a 3:1 ratio. The culture medium was changed 6h later, and virus-containing supernatants were harvested 42h later. Viral particles were filtered, purified by ultracentrifugation through a sucrose cushion (25% weight/volume in Tris-NaCl-EDTA buffer) for 75 min at 4°C and 28,000 rpm using a SW 32 TI rotor (Beckman Coulter), resuspended in serum-free RPMI 1640 or DMEM medium and stored in small aliquots at -80°C. β-lactamase-Vpr (BlaM-Vpr)-carrying viruses, bearing the wild-type Env, were produced by co-transfection of HEK293T cells with the NL4-3/Nef-IRES-Renilla provirus expression vector, pBlaM-Vpr and pAdVAntage at a ratio of 4:1:0.5, as previously described (Cavrois et al., 2002). Viral particles were titrated using an HIV-1 $p24^{Gag}$ Alpha-Lisa kit and an Envision plate reader (Perkin Elmer) and/or by determining their infection titers on target cells.

Lentiviral and retroviral infections. For infections with replication-competent HIV-1 Renilla or wild-type and/or VSV-G pseudotyped-HIV-1, target cells were plated at 2.5 x 10^4 cells per well in 96-well plates or at 2 x 10^5 cells per well in 12-well plates and infected for 24-48 h before lysis and Renilla (and Firefly) luciferase activity measure (Dual-Luciferase® Reporter Assay System Promega) or fixation with 2% paraformaldehyde (PFA)-PBS, permeabilization (Perm/Wash buffer, BDBiosciences) and intracellular staining with the anti-$p24^{Gag}$ KC57-FITC antibody (Beckman

Coulter), as described previously (Goujon and Malim, 2010). For TZM-bl assays, the β-galactosidase activity was measured using the Galacto-Star™ system (ThermoFisher Scientific). For infections with lentiviral and retroviral vectors, target cells were plated at 2.5 x 10^4 cells per well in 96-well plates the day prior to infection with vectors at the indicated MOIs, and the percentages of infected cells were scored by flow cytometry 24h later. For primary CD4+ T cell infections, 10^5 cells were infected with 100 ng $p24^{Gag}$ of HIV-1 Renilla for 24 h prior to lysis and luciferase activity measure. For MDM infections, 8 x 10^4 cells were infected with 100 ng $p24^{Gag}$ of a CCR5-tropic version of HIV-1 Renilla for 30 h prior to lysis and luciferase activity measure.

Retrotransposon assays. For GFP-based retrotransposon assays, HEK293T cells (2 x 10^5 cells) were co-transfected with either 1 µg of pJM111 (a negative control with two point mutations in ORF1 that abolish retrotransposition), pRPS-GFP or pLRE3-GFP with either 1 µg of pCAGGS-Firefly or pCAGGS-DDX42. At 7 days post-transfection, the percentage of GFP-expressing cells was scored by flow cytometry. For endogenous LINE-1 assays, siRNA-transfected U87-MG cells were cultured for 15-21 days prior to RNA extraction and RT-qPCR analysis.

CRISPR/Cas9 knock-out

For CRISPR/Cas9 knock-out in cell lines, Lentiguide-Puro LVs coding sgRNAs targeting the indicated genes or non-targeting sgRNAs were produced, and U87-MG Cas9/CD4/CXCR4/Firefly were transduced for 6 h before replacing the supernatants with fresh, complete medium. The transduced cells were selected with puromycin two days later and amplified for 12-15 day. For CRISPR/Cas9 knock-out in activated primary CD4+ T cells, 2 million cells per condition were washed with PBS1X, and electroporated using the 4d-Nucleofector® (Lonza) and the Amaxa P3 primary cell kit with 183 pmol of crispr/tracr RNA duplex (Alt-R CRISPR-Cas9 crRNA XT and tracrRNA XT, IDT®) and 61 pmol of Cas9 (Alt-R® S.p. Cas9 Nuclease V3, IDT®). After electroporation, the cells were incubated for 4 days at 37°C in X-VIVO15 medium (Lonza) supplemented with 1% pen/strep and IL-2 at 500 U/ml prior to cell counting and infection. The

crRNA sequences of the sgDDX42-1, -2, and -3 were identical to the ones cloned in pLentiguide-Puro, and the crRNA of the sgDDX42-4 and sgDDX42-5 were pre-designed by IDT®, as follow: sg4-DDX42 5'-CGGAGATCTATTAACTGCTG-3', sg5-DDX42 5'-GAGTTGGTGAGTTTTCAGC-3'.

siRNA transfection. DDX42 and control knockdowns were achieved by transfecting the indicated siRNAs at 44nM, 14.2nM, and 100nM final in U87-MG cells, TZM-bl cells and MDMs, respectively, with lipofectamine RNAimax (Thermofisher Scientific) according to the manufacturer's instructions. The scramble siRNA controls used were universal siCTRL1 (SIC001) and siCTRL2 (SIC002) (Sigma-Aldrich) and the sequences of the siRNAs targeting DDX42 were siDDX42-1: 5'-CAGAAUGCCUGGUUUCGGA-3' (SASI_Hs01_00119846, Sigma-Aldrich®), siDDX42-2: 5'-CUUACCUUGUGUUUGAUGA-3' (SASI_Hs01_00119845, Sigma-Aldirch®), siDDX42-4: 5'-AUCUCGAAUACCCUUUACG-3' (ID :136410, Ambion®).

Quantification of mRNA expression. 0,5-2 x 10^6 cells were collected 2-3 days after siRNA transfection or 24h after IFN treatment or no treatment, and total RNAs were isolated using the RNeasy kit with on-column DNase treatment (Qiagen). cDNAs were generated using 250 ng RNA (High-Capacity cDNA Reverse Transcription Kit, Applied Biosystem, ThermoFisher Scientific, catalogue number 4368814) and analysed by quantitative (q)PCR using TaqMan gene expression assays (Applied Biosystem) specific for *ACTB* (Hs99999903_m1), GAPDH (Hs99999905_m1), DDX42 (Hs00201296_m1), and ISG15 (Hs00192713_m1). For the measure of endogenous LINE-1, 1-2 x 10^6 cells were collected 15-20 days after siRNA transfection, total RNAs were isolated and cDNAs were generated using 250 ng RNA as described and analysed by qPCR using the primers and probes specific for *ORF1* and *ORF2*, respectively: ORF1-forward 5'-CTCGGCAGAAACCCTACAAG-3', ORF1-reverse 5'-CCATGTTTAGCGCTTCCTTC-3', with the probe 5'-[FAM]-TTTCAACCCAGAATTTCATATCCAGCCAAAC-[TAMRA]-3', and ORF2-forward 5'-CACCAGTTAGAATGGCAATCATTAAA-3', ORF2-reverse 5'-GGGATGGCTGGGTCAAATGG-3' with the probe 5'-[FAM]-AGGAAACAACAGGTGCTGGAGAGGATGC-[TAMRA]-3. Triplicate reactions were run

according to the manufacturer's instructions using a ViiA 7 Real-Time PCR system. For relative quantification, samples were normalized to both *ACTB* and *GAPDH* mRNA expression and the ΔΔCt analysis. For the measure of SARS-CoV-2 replication, 3 x 10^5 cells were harvested and total RNA was extracted using the RNeasy kit (Qiagen) employing on-column DNase treatment. 125 ng of cellular RNAs were used to generate cDNAs that were analysed by qPCR using RdRp primers and probe, as follow: RdRp_for 5'-GTGARATGGTCATGTGTGGCGG-3', RdRp_rev 5'-CAAATGTTAAAAACACTATTAGCATA-3', and RdRp_probe 5'-[FAM]-CAGGTGGAACCTCATCAGGAGATGC-[TAMRA]-3' (Corman et al., 2020).

BlaM-Vpr assay for HIV-1 entry. These assays were performed as described previously (Goujon and Malim, 2010). Briefly, 2 x 10^5 U87-MG/CD4/CXCR4 cells were plated in 24-well plates and incubated with BlaM-Vpr carrying NL4-3 particles (31, 62, 125 ng $p24^{Gag}$) or mock-infected for 3 h at 37°C. The cells were then washed once in CO_2-independent medium and loaded with CCF2-AM substrate-containing solution (ThermoFisher Scientific) for 1 h at room temperature before 2 washes and incubation at room temperature for 16 h in development medium (CO_2-independent medium containing 2,5 mM probenecid). Finally, the cells were trypsinized, washed and fixed in 1% paraformaldehyde (PFA)-PBS1X before analysis with a FACSCanto™ II (Becton Dickinson).

Quantification of HIV-1 DNAs. To measure HIV-1 cDNAs, 2 x 10^5 cells transfected with a control siRNA or siRNAs targeting DDX42 were plated in 24-well plates, and treated or not with 10 μM AZT and 3TC 1-2 h prior to infection. The cells were infected with NL4-3 HIV-1 (60 ng $p24^{Gag}$) for 2 h at 37°C, washed with PBS1X and incubated in complete DMEM before being harvested at the indicated times. Cell pellets were frozen at -80°C after two washes in PBS1X. Total DNA extraction was performed using the DNeasy kit (Qiagen) according to the manufacturer's instructions, and a DpnI-treatment step was performed prior to qPCR. Strong stop reverse transcription products were detected using forward primer oHC64 5'-TAACTAGGGAACCCACTGC-3' and reverse primer oHC65 5'-GCTAGAGATTTTCCACACTG-3', 1st strand transfer products using forward primer oSA62F 5'-GAGCCCTCAGATGCTGCATAT-

3' and oHC65 as the reverse primer, 2nd strand transfer product using oHC64 and oSA63R 5'-CTGCGTCGAGAGATCTCCTCTGGCT-3', together with oHC66 probe 5'-[FAM]-ACACAACAGACGGGCACACACTA-[TAMRA]-3'. 2-LTR circular forms were detected using 2LTR-forward 5'-GTAACTAGAGATCCCTCAG-3' and 2LTR-reverse 5'-TGGCCCTGGTGTGTAGTTC-3' together with 2LTR-probe 5′-[FAM]-CTACCACACACAAGGCTACTTCCCTGAT-[TAMRA]-3'. Integrated viral DNA was analysed using an Alu qPCR as described before (Goujon et al., 2013a). Briefly, a preamplification of 16 cycles was performed (15 sec at 94°C, 15 sec at 55°C, 100 sec at 68°C) with Platinum Taq DNA High Fidelity polymerase (Invitrogen) using 100 nM of genomic Alu forward primer 5′-GCCTCCCAAAGTGCTGGGATTACAG and 600 nM of U3-reverse primer 5'-CTTCTACCTTATCTGGCTCAAC-3'. The pre-amplification step was performed on serial dilutions of all the DNA samples, as well as of a positive control (total DNA from U87-MG infected with a high input of NL4-3), to ensure the linearity of the assay. Background levels were assessed using linear, one-way amplification by performing the pre-amplification PCR with the U3-reverse primer alone. Then a qPCR was performed on pre-amplification products using U3-forward primer 5'-TCTACCACACACAAGGCTAC-3' and U3-reverse primer with the U3 probe 5'-[FAM]-CAGAACTACACACCAGGGCCAGGGGTCA-[TAMRA]-3'. qPCR reactions were performed in triplicates, in Universal PCR master mix using 900nM each primer and 250nM probe with the following program: 10 min at 95°C followed by 40 cycles (15 sec at 95°C and 1 min at 60°C). pNL4-3 or pTOPO-2LTR (generated by pTOPO cloning of a 2-LTR circle junction amplified from NL4-3 infected cells, using oHC64 and U3-reverse primers into pCR™2.1-TOPO™) were diluted in 20 ng/ml of salmon sperm DNA to create dilution standards used to quantify relative cDNA copy numbers and confirm the linearity of all assays.

Proximity Ligation assay. The proximity ligation assays were performed using the Duolink® in situ Detection Reagents (Sigma-Aldrich, DUO92014). For this, MDMs were plated in 24-well plates with coverslips pre-treated with poly-L-lysin (Sigma-Aldrich) and infected with 1 μg $p24^{Gag}$ of HIV-1 NL4-3 (Ba-L Env) or mock-infected. 24 h later, the cells were fixed with 4%

paraformaldehyde in PBS1X for 10 min, washed in PBS1X and permeabilized with 0.2% Triton X-100 for 10 min. After a couple of washes in PBS1X, either NGB buffer (50 mM NH_4Cl, 2% goat serum and 2% bovine serum albumin in PBS) or Duolink® blocking solution was added for 1h. Cells were incubated with AG3.0 mouse anti-Capsid antibody obtained from the National Institutes of Health (NIH) AIDS Reagent Program (#4121) and anti-DDX42 rabbit antibody (HPA023571, Sigma-Aldrich) diluted in NGB buffer or in Duolink® blocking solution for 1h. After 2 washes in PBS1X, the cells were incubated with the DUOLINK® in situ PLA® Probe Anti-rabbit minus (DUO92006) and DUOLINK® in situ PLA® Probe Anti-mouse plus (DUO92001) for 1h at 37°C. After 2 washes in PBS1X, the ligation mix was added for 30 min at 37°C. After 2 washes in PBS1X, the cells were incubated with the amplification mix for 100 min at 37°C. Finally, the cells were washed twice with PBS1X and stained with Hoechst at 1 μg/mL for 5 min, washed again and the coverslips mounted on slides in Prolong mounting media (ThermoFisher Scientific). Z-stack images were acquired using an LSM 880 confocal microscope (ZEISS) using a 63x lens. PLA punctae quantification was performed using the FIJI software (Schindelin et al., 2012). Briefly, maximum z-projections were performed on each z-stack and the number of nuclei per field were quantified. Then, by using a median filter and thresholding, PLA punctae were isolated and quantified automatically using the Analyse Particles function. To obtain a mean number of dots per cell, the number of PLA dots per field were averaged by the number of nuclei. For representative images, single cells were imaged using a LSM880 confocal microscope coupled with an Airyscan module. Processing of the raw Airyscan images was performed on the ZEN Black software.

Immunoblot analysis. Cell pellets were lysed in sample buffer (200 mM Tris-HCl, pH 6.8, 5.2% SDS, 20% glycerol, 0.1% bromophenol blue, 5% β-mercaptoethanol), resolved by SDS–PAGE and analysed by immunoblotting using primary antibodies specific for human DDX42 (HPA023571, Sigma-Aldrich) and Actin (mouse monoclonal A1978, Sigma-Aldrich), followed by secondary horseradish peroxidase-conjugated anti-mouse or anti-rabbit immunoglobulin

antibodies and chemiluminescence (Bio-Rad). Images were acquired on a ChemiDoc™ gel imaging system (Bio-Rad).

IAV production and infection

We have described previously IAV NanoLuciferase reporter virus generation (Doyle et al., 2018). Stocks were titrated by plaque assays on MDCK cells. IAV challenges were performed in serum-free DMEM for 1 h and the medium was subsequently replaced with DMEM containing 10%. IAV infection experiments were performed in triplicates in 96-well plates with cultures maintained for 16 h post-challenge. NanoLuciferase activity was measured with the Nano-Glo assay system (Promega), and luminescence was detected using a plate reader (Infinite® 200 PRO, Tecan).

VSV production and infection. A VSV-G pseudotyped-VSV-Δenv reporter virus, coding both GFP and Firefly Luciferase, was obtained from Gert Zimmer (Rentsch and Zimmer, 2011). The virus was amplified on pMD.G transfected 293T and titrated thanks to the GFP reporter gene. For infection, 2.5 x 10^4 cells per well in 96-well plates were infected at the indicated MOIs. 24h after infection, cells were lysed and Firefly luciferase activity was measured (Firefly luciferase Assay System Promega).

ZIKV production and infection. The nanoluciferase expressing ZIKV construct has been described (Mutso et al., 2017). The corresponding linearized plasmid was transcribed in vitro using the SP6 mMESSAGE mMACHINE™ (Thermofischer Scientific) and HEK293T cells were transfected with the transcribed RNA. After 7 days, supernatants were harvested, filtered and stock titers were determined by plaque assays on Vero cells. For infections, 2.5 x 10^4 cells per well in 96-well plates were infected, at the indicated MOIs. 24h after infection, cells were lysed and Nanoluciferase activity was measured using the Kit Nano Glo luciferase Assay (Promega).

CHIKV production and infection. The Gaussi luciferase coding CHIKV construct has been described (Pohjala et al., 2011). The linearized plasmid coding CHIKV genome was transcribed

with the T7 mMESSAGE mMACHINE kit (Thermofischer Scientific) and 5 x 10^5 HEK293T were transfected with 1-4 μg of transcribed RNA, using Lipofectamine 2000 (Thermofischer Scientific). After 24h, supernatants were harvested, filtered and viruses were then amplified on baby hamster kidney (BHK21) cells. Stock titers were determined by plaque assays on Vero cells. For infections, 2.5 x 10^4 cells per well in 96-well plates were infected at the indicated MOIs. 24h after infection, cells were lysed and Gaussia luciferase activity was measured using the Pierce™ Gaussia Luciferase Flash Assay Kit (Thermofischer Scientific).

SARS-CoV-2 production and infection

The SARS-CoV-2 BetaCoV/France/IDF0372/2020 isolate was supplied by Pr. Sylvie van der Werf and the National Reference Centre for Respiratory Viruses hosted by Institut Pasteur (Paris, France). The virus was amplified in Vero E6 cells (MOI 0,005) in serum-free media supplemented with 0,1 μg/ml L-1-p-Tosylamino-2-phenylethyl chloromethylketone (TPCK)-treated trypsin (Sigma-Aldrich). The supernatant was harvested at 72 h post infection when cytopathic effects were observed (with around 50% cell death), cell debris were removed by centrifugation, and aliquots stored at -80C. Viral supernatants were titrated by plaque assays in Vero E6 cells. Typical titers were 5.10^6 plaque forming units (PFU)/ml.

Infections of A549-ACE2 cells were performed at the indicated multiplicity of infection (MOI; as calculated from titers obtained in Vero E6 cells) in serum-free DMEM and 5% serum-containing DMEM, respectively. The viral input was left for the duration of the experiment and cells lysed at 48 h post-infection for RT-qPCR analysis.

Data availability

The datasets generated during and/or analysed during the current study are available from the corresponding authors on reasonable request.

Requests for materials

Requests for material should be addressed to Caroline Goujon or Olivier Moncorgé at the corresponding address above, or to Addgene for the plasmids with an Addgene number.

Acknowledgements

We wish to thank Tom Doyle and Chad Swanson for their useful comments on the manuscript, and Matthieu Lewis, Nadine Laguette, Emiliano Ricci, Nathalie Arhel, Juliette Fernandez, Jean-Luc Battini, Georg Kochs and Nathan Sherer for the generous provision of reagents, protocols and/or for helpful discussions. We are grateful to Nicolas Manel and Helena Izquierdo-Fernandez for providing us their protocol for efficient knockdown in primary CD4+ T cell using CRISPR/Cas9 RNP electroporation. We are grateful to Myriam Boyer, Stéphanie Viala, Baptiste Monterroso and Orestis Faklaris from the imaging and flow cytometry facility MRI, for advice with flow cytometry and confocal microscopy, respectively. This work was supported by the Institut National de la Santé et de la Recherche Médicale (INSERM) (to CG), the ATIP-Avenir programme (to CG), institutional funds from the Centre National de la Recherche Scientifique (CNRS) and Montpellier University, France REcherche Nord&Sud Sida/HIV et Hépatites (ANRS) (ECTZ21792 to CG; ECTZ35478 to OM), Sidaction (to CG), a Starting Grant from the European Research Council (759226, ANTIViR) (to CG), PhD studentships from the Ministry of Higher Education and Research (to BB, JM and AR), and a 4th year PhD studentship from the Fondation pour la Recherche Médicale (to BB). SR and HP acknowledge financial support from the France Génomique National infrastructure, funded as part of “Investissement d’Avenir” program managed by Agence Nationale de la Recherche (contract ANR-10-INBS-09). We acknowledge the imaging facility MRI, member of the national infrastructure France-BioImaging supported by the French National Research Agency (ANR-10-INBS-04).

Author contributions

B.B. and CG designed the study, analysed the data and wrote the manuscript. B.B. and C.G. performed the whole-genome screens and candidate validation. B.B. carried out most of the experiments, with technical assistance from A.R., F.G.d.G, M.T., J.M., W.D., A.M., and O.M.; V.C. provided some of the lentiviral vector stocks. H.P. and S.R. performed the Illumina sequencing and MaGECK analyses, respectively. All authors have read and approved the manuscript.

Conflicts of interest statement

The authors have no conflicts of interest to declare in relation to this manuscript.

References

Adachi, A., Gendelman, H.E., Koenig, S., Folks, T., Willey, R., Rabson, A., and Martin, M.A. (1986). Production of acquired immunodeficiency syndrome-associated retrovirus in human and nonhuman cells transfected with an infectious molecular clone. J. Virol. *59*, 284–291.

Baca-Regen, L., Heinzinger, N., Stevenson, M., and Gendelman, H.E. (1994). Alpha interferon-induced antiretroviral activities: restriction of viral nucleic acid synthesis and progeny virion production in human immunodeficiency virus type 1-infected monocytes. J. Virol. *68*, 7559–7565.

Bainbridge, J.W., Stephens, C., Parsley, K., Demaison, C., Halfyard, A., Thrasher, A.J., and Ali, R.R. (2001). In vivo gene transfer to the mouse eye using an HIV-based lentiviral vector; efficient long-term transduction of corneal endothelium and retinal pigment epithelium. Gene Ther. *8*, 1665–1668.

Bednarik, D.P., Mosca, J.D., Raj, N.B., and Pitha, P.M. (1989). Inhibition of human immunodeficiency virus (HIV) replication by HIV-trans-activated alpha 2-interferon. Proc. Natl. Acad. Sci. U. S. A. *86*, 4958–4962.

Belancio, V.P., Roy-Engel, A.M., Pochampally, R.R., and Deininger, P. (2010). Somatic expression of LINE-1 elements in human tissues. Nucleic Acids Res. *38*, 3909–3922.

Branciforte, D., and Martin, S.L. (1994). Developmental and cell type specificity of LINE-1 expression in mouse testis: implications for transposition. Mol. Cell. Biol. *14*, 2584–2592.

Bulli, L., Apolonia, L., Kutzner, J., Pollpeter, D., Goujon, C., Herold, N., Schwarz, S.-M., Giernat, Y., Keppler, O.T., Malim, M.H., et al. (2016). Complex interplay between HIV-1 Capsid and MX2-independent IFNα-induced antiviral factors. J. Virol.

Burdick, R.C., Li, C., Munshi, M., Rawson, J.M.O., Nagashima, K., Hu, W.-S., and Pathak, V.K. (2020). HIV-1 uncoats in the nucleus near sites of integration. Proc. Natl. Acad. Sci. *117*, 5486–5493.

Cavrois, M., de Noronha, C., and Greene, W.C. (2002). A sensitive and specific enzyme-based assay detecting HIV-1 virion fusion in primary T lymphocytes. Nat. Biotechnol. *20*, 1151–1154.

Cheney, K.M., and McKnight, Á. (2010). Interferon-alpha mediates restriction of human immunodeficiency virus type-1 replication in primary human macrophages at an early stage of replication. PloS One *5*, e13521.

Coccia, E.M., Krust, B., and Hovanessian, A.G. (1994). Specific inhibition of viral protein synthesis in HIV-infected cells in response to interferon treatment. J. Biol. Chem. *269*, 23087–23094.

Corman, V.M., Landt, O., Kaiser, M., Molenkamp, R., Meijer, A., Chu, D.K., Bleicker, T., Brünink, S., Schneider, J., Schmidt, M.L., et al. (2020). Detection of 2019 novel coronavirus (2019-nCoV) by real-time RT-PCR. Euro Surveill. Bull. Eur. Sur Mal. Transm. Eur. Commun. Dis. Bull. *25*.

Dharan, A., Bachmann, N., Talley, S., Zwikelmaier, V., and Campbell, E.M. (2020). Nuclear pore blockade reveals that HIV-1 completes reverse transcription and uncoating in the nucleus. Nat. Microbiol.

Doench, J.G. (2018). Am I ready for CRISPR? A user's guide to genetic screens. Nat. Rev. Genet. *19*, 67–80.

Doyle, T., Goujon, C., and Malim, M.H. (2015). HIV-1 and interferons: who's interfering with whom? Nat. Rev. Microbiol. *13*, 403–413.

Doyle, T., Moncorgé, O., Bonaventure, B., Pollpeter, D., Lussignol, M., Tauziet, M., Apolonia, L., Catanese, M.-T., Goujon, C., and Malim, M.H. (2018). The interferon-inducible isoform of NCOA7 inhibits endosome-mediated viral entry. Nat. Microbiol. *3*, 1369–1376.

Ergün, S., Buschmann, C., Heukeshoven, J., Dammann, K., Schnieders, F., Lauke, H., Chalajour, F., Kilic, N., Strätling, W.H., and Schumann, G.G. (2004). Cell Type-specific Expression of LINE-1 Open Reading Frames 1 and 2 in Fetal and Adult Human Tissues. J. Biol. Chem. *279*, 27753–27763.

Fay, M.M., Lyons, S.M., and Ivanov, P. (2017). RNA G-Quadruplexes in Biology: Principles and Molecular Mechanisms. J. Mol. Biol. *429*, 2127–2147.

Gaddis, N.C., Sheehy, A.M., Ahmad, K.M., Swanson, C.M., Bishop, K.N., Beer, B.E., Marx, P.A., Gao, F., Bibollet-Ruche, F., Hahn, B.H., et al. (2004). Further Investigation of Simian Immunodeficiency Virus Vif Function in Human Cells. J. Virol. *78*, 12041–12046.

Ghimire, D., Rai, M., and Gaur, R. (2018). Novel host restriction factors implicated in HIV-1 replication. J. Gen. Virol. *99*, 435–446.

Gilbert, N., Lutz, S., Morrish, T.A., and Moran, J.V. (2005). Multiple Fates of L1 Retrotransposition Intermediates in Cultured Human Cells. Mol. Cell. Biol. *25*, 7780–7795.

Goodier, J.L., Cheung, L.E., and Kazazian, H.H. (2012). MOV10 RNA Helicase Is a Potent Inhibitor of Retrotransposition in Cells. PLoS Genet. *8*, e1002941.

Goujon, C., and Malim, M.H. (2010). Characterization of the alpha interferon-induced postentry block to HIV-1 infection in primary human macrophages and T cells. J. Virol. *84*, 9254–9266.

Goujon, C., Arfi, V., Pertel, T., Luban, J., Lienard, J., Rigal, D., Darlix, J.-L., and Cimarelli, A. (2008). Characterization of Simian Immunodeficiency Virus SIVSM/Human Immunodeficiency Virus Type 2 Vpx Function in Human Myeloid Cells. J. Virol. *82*, 12335–12345.

Goujon, C., Moncorgé, O., Bauby, H., Doyle, T., Ward, C.C., Schaller, T., Hué, S., Barclay, W.S., Schulz, R., and Malim, M.H. (2013a). Human MX2 is an interferon-induced post-entry inhibitor of HIV-1 infection. Nature *502*, 559–562.

Goujon, C., Schaller, T., Galão, R.P., Amie, S.M., Kim, B., Olivieri, K., Neil, S.J.D., and Malim, M.H. (2013b). Evidence for IFNα-induced, SAMHD1-independent inhibitors of early HIV-1 infection. Retrovirology *10*, 23.

Granneman, S., Bernstein, K.A., Bleichert, F., and Baserga, S.J. (2006). Comprehensive Mutational Analysis of Yeast DEXD/H Box RNA Helicases Required for Small Ribosomal Subunit Synthesis. Mol. Cell. Biol. *26*, 1183–1194.

Gringhuis, S.I., Hertoghs, N., Kaptein, T.M., Zijlstra-Willems, E.M., Sarrami-Forooshani, R., Sprokholt, J.K., van Teijlingen, N.H., Kootstra, N.A., Booiman, T., van Dort, K.A., et al. (2017). HIV-1 blocks the signaling adaptor MAVS to evade antiviral host defense after sensing of abortive HIV-1 RNA by the host helicase DDX3. Nat. Immunol. *18*, 225–235.

Haller, O., Staeheli, P., Schwemmle, M., and Kochs, G. (2015). Mx GTPases: dynamin-like antiviral machines of innate immunity. Trends Microbiol. *23*, 154–163.

Ho, D.D., Hartshorn, K.L., Rota, T.R., Andrews, C.A., Kaplan, J.C., Schooley, R.T., and Hirsch, M.S. (1985). Recombinant human interferon alfa-A suppresses HTLV-III replication in vitro. Lancet Lond. Engl. *1*, 602–604.

Jimenez-Guardeño, J.M., Apolonia, L., Betancor, G., and Malim, M.H. (2019). Immunoproteasome activation enables human TRIM5α restriction of HIV-1. Nat. Microbiol.

Kane, M., Yadav, S.S., Bitzegeio, J., Kutluay, S.B., Zang, T., Wilson, S.J., Schoggins, J.W., Rice, C.M., Yamashita, M., Hatziioannou, T., et al. (2013). MX2 is an interferon-induced inhibitor of HIV-1 infection. Nature *502*, 563–566.

Langmead, B., Trapnell, C., Pop, M., and Salzberg, S.L. (2009). Ultrafast and memory-efficient alignment of short DNA sequences to the human genome. Genome Biol. *10*, R25.

Li, H., Handsaker, B., Wysoker, A., Fennell, T., Ruan, J., Homer, N., Marth, G., Abecasis, G., Durbin, R., and 1000 Genome Project Data Processing Subgroup (2009). The Sequence Alignment/Map format and SAMtools. Bioinforma. Oxf. Engl. *25*, 2078–2079.

Li, W., Xu, H., Xiao, T., Cong, L., Love, M.I., Zhang, F., Irizarry, R.A., Liu, J.S., Brown, M., and Liu, X.S. (2014). MAGeCK enables robust identification of essential genes from genome-scale CRISPR/Cas9 knockout screens. Genome Biol. *15*, 554.

Liu, N., Lee, C.H., Swigut, T., Grow, E., Gu, B., Bassik, M.C., and Wysocka, J. (2018). Selective silencing of euchromatic L1s revealed by genome-wide screens for L1 regulators. Nature *553*, 228–232.

Liu, Z., Pan, Q., Liang, Z., Qiao, W., Cen, S., and Liang, C. (2015). The highly polymorphic cyclophilin A-binding loop in HIV-1 capsid modulates viral resistance to MxB. Retrovirology *12*, 1.

Martin, M. (2011). Cutadapt removes adapter sequences from high-throughput sequencing reads. EMBnet.Journal *17*, 10–12.

Moncorge, O., Long, J.S., Cauldwell, A.V., Zhou, H., Lycett, S.J., and Barclay, W.S. (2013). Investigation of Influenza Virus Polymerase Activity in Pig Cells. J. Virol. *87*, 384–394.

Moran, J.V., Holmes, S.E., Naas, T.P., DeBerardinis, R.J., Boeke, J.D., and Kazazian, H.H. (1996). High frequency retrotransposition in cultured mammalian cells. Cell *87*, 917–927.

Muotri, A.R., Chu, V.T., Marchetto, M.C.N., Deng, W., Moran, J.V., and Gage, F.H. (2005). Somatic mosaicism in neuronal precursor cells mediated by L1 retrotransposition. Nature *435*, 903–910.

Mutso, M., Saul, S., Rausalu, K., Susova, O., Žusinaite, E., Mahalingam, S., and Merits, A. (2017). Reverse genetic system, genetically stable reporter viruses and packaged subgenomic replicon based on a Brazilian Zika virus isolate. J. Gen. Virol. *98*, 2712–2724.

Naldini, L., Blömer, U., Gallay, P., Ory, D., Mulligan, R., Gage, F.H., Verma, I.M., and Trono, D. (1996). In vivo gene delivery and stable transduction of nondividing cells by a lentiviral vector. Science *272*, 263–267.

Ochsenbauer, C., Edmonds, T.G., Ding, H., Keele, B.F., Decker, J., Salazar, M.G., Salazar-Gonzalez, J.F., Shattock, R., Haynes, B.F., Shaw, G.M., et al. (2012). Generation of transmitted/founder HIV-1 infectious molecular clones and characterization of their replication capacity in CD4 T lymphocytes and monocyte-derived macrophages. J. Virol. *86*, 2715–2728.

OhAinle, M., Helms, L., Vermeire, J., Roesch, F., Humes, D., Basom, R., Delrow, J.J., Overbaugh, J., and Emerman, M. (2018). A virus-packageable CRISPR screen identifies host factors mediating interferon inhibition of HIV. ELife *7*.

O'Rourke, J.P., Newbound, G.C., Kohn, D.B., Olsen, J.C., and Bunnell, B.A. (2002). Comparison of gene transfer efficiencies and gene expression levels achieved with equine infectious anemia virus- and human immunodeficiency virus type 1-derived lentivirus vectors. J. Virol. *76*, 1510–1515.

Ostertag, E.M., Prak, E.T., DeBerardinis, R.J., Moran, J.V., and Kazazian, H.H. (2000). Determination of L1 retrotransposition kinetics in cultured cells. Nucleic Acids Res. *28*, 1418–1423.

Peng, K., Muranyi, W., Glass, B., Laketa, V., Yant, S.R., Tsai, L., Cihlar, T., Müller, B., and Kräusslich, H.-G. (2014). Quantitative microscopy of functional HIV post-entry complexes reveals association of replication with the viral capsid. ELife *3*, e04114.

Pohjala, L., Utt, A., Varjak, M., Lulla, A., Merits, A., Ahola, T., and Tammela, P. (2011). Inhibitors of Alphavirus Entry and Replication Identified with a Stable Chikungunya Replicon Cell Line and Virus-Based Assays. PLOS ONE *6*, e28923.

Rangwala, S.H., Zhang, L., and Kazazian, H.H. (2009). Many LINE1 elements contribute to the transcriptome of human somatic cells. Genome Biol. *10*, R100.

Rentsch, M.B., and Zimmer, G. (2011). A Vesicular Stomatitis Virus Replicon-Based Bioassay for the Rapid and Sensitive Determination of Multi-Species Type I Interferon. PLoS ONE *6*.

Rocak, S. (2005). Characterization of the ATPase and unwinding activities of the yeast DEAD-box protein Has1p and the analysis of the roles of the conserved motifs. Nucleic Acids Res. *33*, 999–1009.

Ruggiero, E., and Richter, S.N. (2018). G-quadruplexes and G-quadruplex ligands: targets and tools in antiviral therapy. Nucleic Acids Res. *46*, 3270–3283.

Ryan-Graham, M.A., and Peden, K.W.C. (1995). Both Virus and Host Components Are Important for the Manifestation of a Nef- Phenotype in HIV-1 and HIV-2. Virology *213*, 158–168.

Saenz, D.T., Teo, W., Olsen, J.C., and Poeschla, E.M. (2005). Restriction of feline immunodeficiency virus by Ref1, Lv1, and primate TRIM5alpha proteins. J. Virol. *79*, 15175–15188.

Sanjana, N.E., Shalem, O., and Zhang, F. (2014). Improved vectors and genome-wide libraries for CRISPR screening. Nat. Methods *11*, 783–784.

Schaller, T., Ocwieja, K.E., Rasaiyaah, J., Price, A.J., Brady, T.L., Roth, S.L., Hué, S., Fletcher, A.J., Lee, K., KewalRamani, V.N., et al. (2011). HIV-1 capsid-cyclophilin interactions determine nuclear import pathway, integration targeting and replication efficiency. PLoS Pathog. *7*, e1002439.

Schindelin, J., Arganda-Carreras, I., Frise, E., Kaynig, V., Longair, M., Pietzsch, T., Preibisch, S., Rueden, C., Saalfeld, S., Schmid, B., et al. (2012). Fiji: an open-source platform for biological-image analysis. Nat. Methods *9*, 676–682.

Shalem, O., Sanjana, N.E., Hartenian, E., Shi, X., Scott, D.A., Mikkelsen, T.S., Heckl, D., Ebert, B.L., Root, D.E., Doench, J.G., et al. (2014). Genome-scale CRISPR-Cas9 knockout screening in human cells. Science *343*, 84–87.

Shalem, O., Sanjana, N.E., and Zhang, F. (2015). High-throughput functional genomics using CRISPR-Cas9. Nat. Rev. Genet. *16*, 299–311.

Simon, J.H., Southerling, T.E., Peterson, J.C., Meyer, B.E., and Malim, M.H. (1995). Complementation of vif-defective human immunodeficiency virus type 1 by primate, but not nonprimate, lentivirus vif genes. J. Virol. *69*, 4166–4172.

Sithole, N., Williams, C.A., Vaughan, A.M., Kenyon, J.C., and Lever, A.M.L. (2018). DDX17 Specifically, and Independently of DDX5, Controls Use of the HIV A4/5 Splice Acceptor Cluster and Is Essential for Efficient Replication of HIV. J. Mol. Biol. *430*, 3111–3128.

Sithole, N., Williams, C.A., Abbink, T.E.M., and Lever, A.M.L. (2020). DDX5 potentiates HIV-1 transcription as a co-factor of Tat. Retrovirology *17*, 6.

Soto-Rifo, R., Rubilar, P.S., and Ohlmann, T. (2013). The DEAD-box helicase DDX3 substitutes for the cap-binding protein eIF4E to promote compartmentalized translation initiation of the HIV-1 genomic RNA. Nucleic Acids Res. *41*, 6286–6299.

Trelogan, S.A., and Martin, S.L. (1995). Tightly regulated, developmentally specific expression of the first open reading frame from LINE-1 during mouse embryogenesis. Proc. Natl. Acad. Sci. U. S. A. *92*, 1520–1524.

Uhlmann-Schiffler, H., Jalal, C., and Stahl, H. (2006). Ddx42p--a human DEAD box protein with RNA chaperone activities. Nucleic Acids Res. *34*, 10–22.

Uhlmann-Schiffler, H., Kiermayer, S., and Stahl, H. (2009). The DEAD box protein Ddx42p modulates the function of ASPP2, a stimulator of apoptosis. Oncogene *28*, 2065–2073.

Wei, J., Alfajaro, M.M., DeWeirdt, P.C., Hanna, R.E., Lu-Culligan, W.J., Cai, W.L., Strine, M.S., Zhang, S.-M., Graziano, V.R., Schmitz, C.O., et al. (2020). Genome-wide CRISPR screens reveal host factors critical for SARS-CoV-2 infection. Cell.

Will, C.L., Urlaub, H., Achsel, T., Gentzel, M., Wilm, M., and Lührmann, R. (2002). Characterization of novel SF3b and 17S U2 snRNP proteins, including a human Prp5p homologue and an SF3b DEAD-box protein. EMBO J. *21*, 4978–4988.

Williams, C.A., Abbink, T.E.M., Jeang, K.-T., and Lever, A.M.L. (2015). Identification of RNA helicases in human immunodeficiency virus 1 (HIV-1) replication - a targeted small interfering RNA library screen using pseudotyped and WT HIV-1. J. Gen. Virol. *96*, 1484–1489.

Wingett, S.W., and Andrews, S. (2018). FastQ Screen: A tool for multi-genome mapping and quality control. F1000Research *7*, 1338.

Xu, B., Pan, Q., and Liang, C. (2018). Role of MxB in Alpha Interferon-Mediated Inhibition of HIV-1 Infection. J. Virol. *92*.

Yedavalli, V.S.R.K., Neuveut, C., Chi, Y., Kleiman, L., and Jeang, K.-T. (2004). Requirement of DDX3 DEAD Box RNA Helicase for HIV-1 Rev-RRE Export Function. Cell *119*, 381–392.

Zyner, K.G., Mulhearn, D.S., Adhikari, S., Martínez Cuesta, S., Di Antonio, M., Erard, N., Hannon, G.J., Tannahill, D., and Balasubramanian, S. (2019). Genetic interactions of G-quadruplexes in humans. ELife *8*, e46793.

Supplementary Information

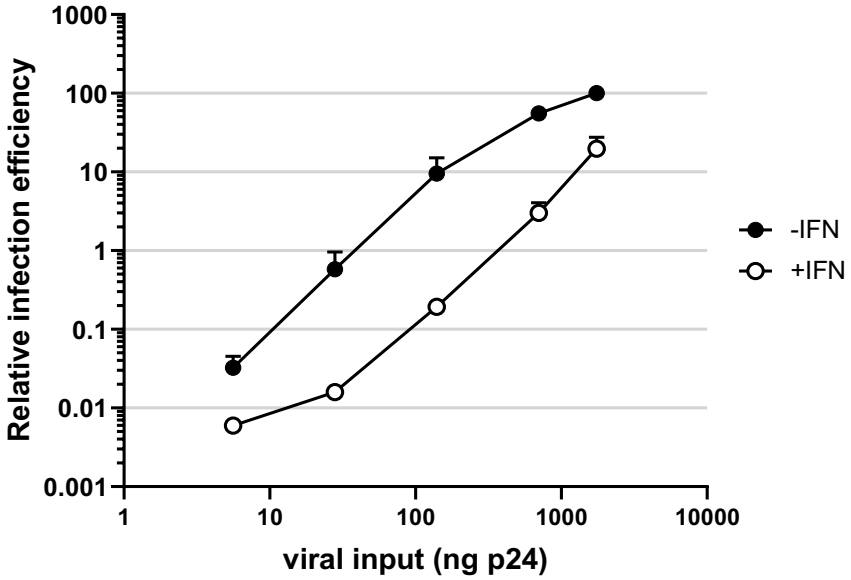

Supplementary Information Figure 1. IFN pre-treatment potently inhibits HIV-1 infection in T98G/CD4/CXCR4 cells, but is at least partially saturable. T98G Cas9/CD4/CXCR4/Firefly cells were pre-treated with IFN for 24 h prior to infection with increasing doses of NL4-3 Renilla (indicated in ng $p24^{Gag}$). Renilla activity was normalized to Firefly activity and the relative infection efficiencies are shown. Data represent the mean ± S.E.M of three independent experiments.

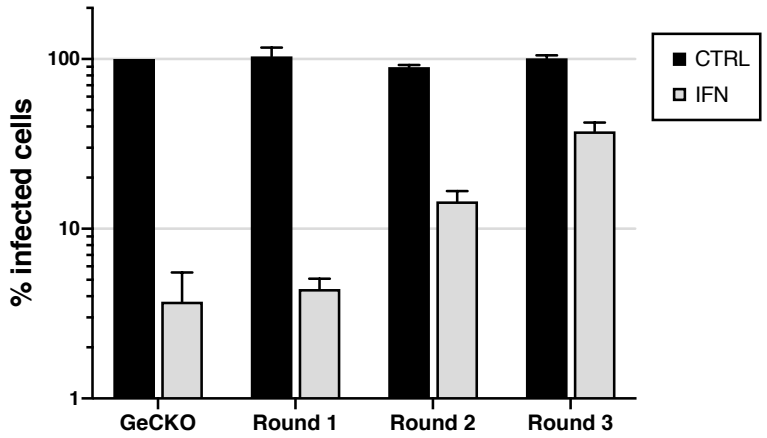

Supplementary Information Figure 2. GeCKO screen validation: the enriched cells become progressively less restrictive to HIV-1 infection following IFN treatment after each round. GeCKO control cells and enriched cells from 3 successive rounds of selection were treated with IFN and infected with GFP-expressing lentiviral vectors. The percentage of infected cells was evaluated by flow cytometry 2 days post-infection. Data represent the average of 2 independent experiments and one standard deviation from the mean.

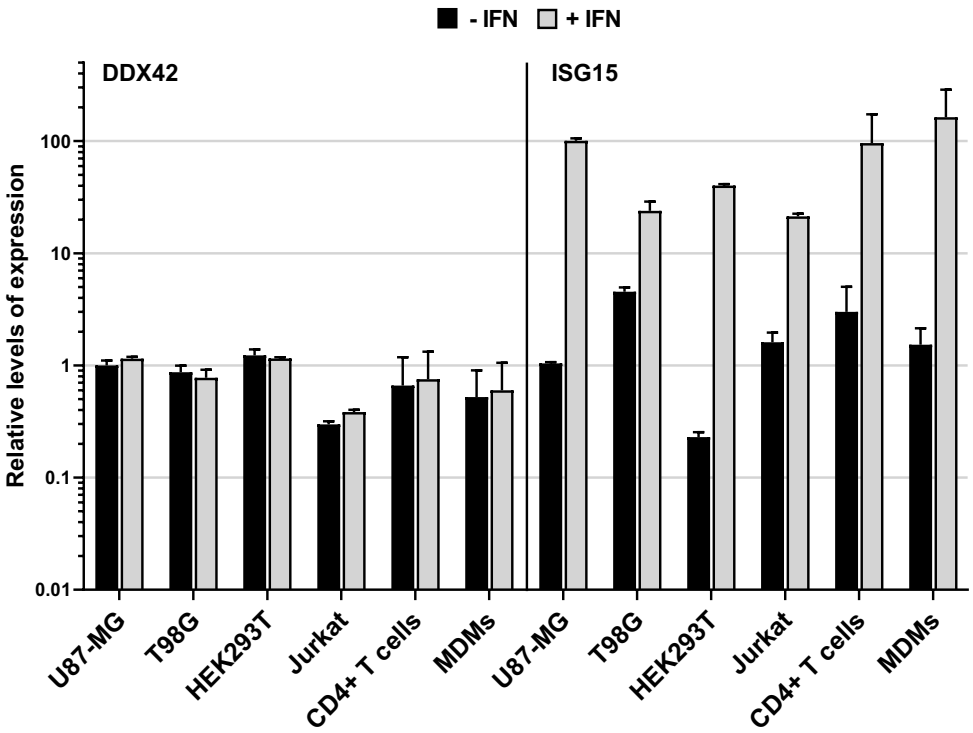

Supplementary Information Figure 3. DDX42 is not an ISG. The indicated primary cells or immortalized cell cultures were treated with IFN for 24 h or left untreated. RNA was subsequently extracted and DDX42 and ISG15 (a prototype ISG) mRNA levels were quantified by RT-qPCR; Actin B and GAPDH were used as endogenous controls. The bar chart shows the relative levels of expression of DDX42 and ISG15 in the presence or absence of IFN treatment. Data represent the mean ± S.E.M of three independent experiments.

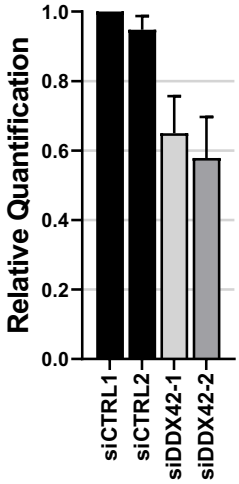

Supplementary Information Figure 4. DDX42 silencing efficiency in monocyte-derived macrophages. siRNA-transfected MDMs were harvested 48h post-transfection for RNA extraction and quantification of DDX42 mRNA levels by RT-qPCR. Actin and GAPDH were used as endogenous controls. Data represent the mean ± S.E.M of three independent experiments performed with cells from 3 different blood donors.

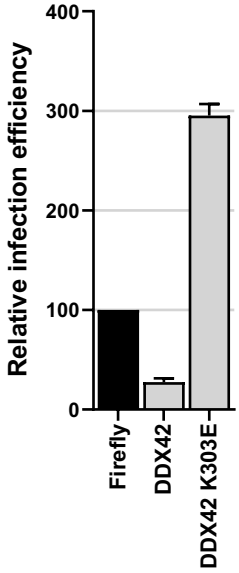

Supplementary Information Figure 5. Ectopic expression of DDX42 K303E mutant increases HIV-1 infection. U87-MG/CD4/CXCR4 cells were transduced with lentiviral vectors expressing either Firefly (negative control), WT DDX42 (DDX42) or a motif I mutant DDX42 K303, which has an impaired ATPase activity (DDX42 K303E). Transduced cells were infected with NL4-3 Renilla and the infection efficiency was assessed 24h later by measuring the Renilla activity. Data represent the mean ± S.E.M of four independent experiments.

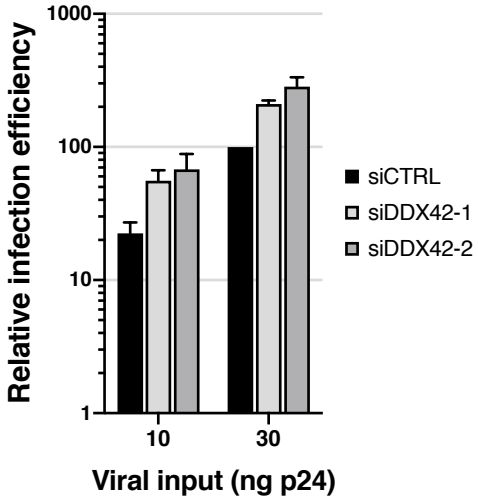

Supplementary Information Figure 6. Endogenous DDX42 inhibits VSV-G-pseudotyped HIV-1 Renilla. siRNA transfected-U87-MG/CD4/CXCR4 cells were infected with the indicated amounts of VSV-G pseudotyped HIV-1 Renilla. The infection efficiency was assessed 18h later by monitoring Renilla activity. Data represent the mean ± S.E.M of three independent experiments.

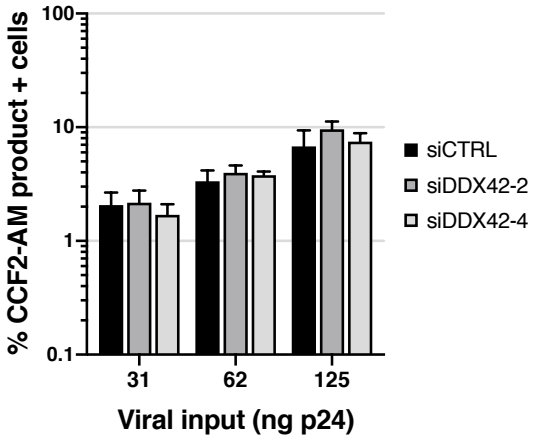

Supplementary Information Figure 7. DDX42 depletion does not affect HIV-1 entry. DDX42-depleted U87-MG/CD4/CXCR4 cells were infected with the indicated amounts of viruses carrying the β-lactamase (BlaM)-Vpr fusion protein for 3 hours. The cells were subsequently loaded with CCF2-AM substrate dye for 2h, washed extensively and incubated for another 16h for the reaction to develop. Cells positive for the CCF2-AM product were scored by flow cytometry. Data represent the mean ± S.E.M of three independent experiments.

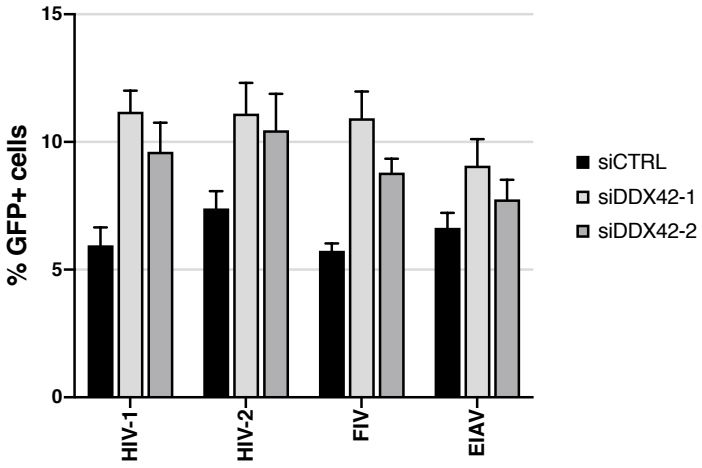

Supplementary Information Figure 8. U87-MG/CD4/CXCR4 cells were transfected with non-targeting siRNA (siCTRL) or siRNAs targeting DDX42 (siDDX42-1, -2, and -4) and, 72 h later, the cells infected with HIV-1- HIV-2- FIV- EIAV-based, GFP-coding LVs at an MOI of 0,1. Infection efficiency was scored 24 h by measuring the percentage of GFP expressing cells by flow cytometry. Data represent the mean ± S.E.M of three independent experiments.

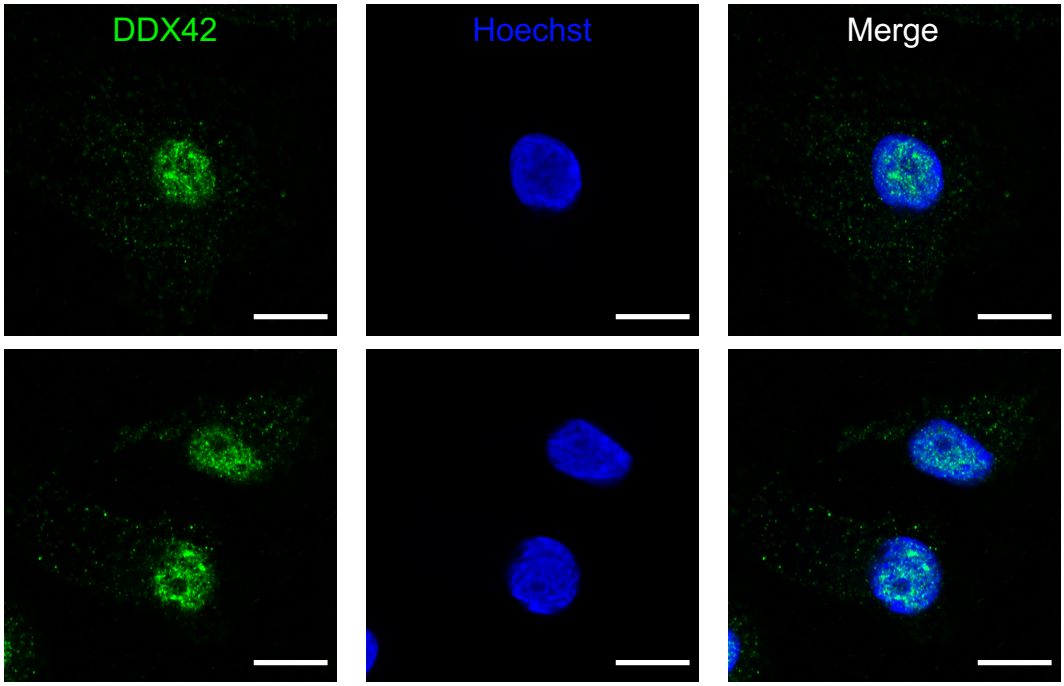

Supplementary Information Figure 9. Indirect immunofluorescence analysis of endogenous DDX42 in primary MDMs. MDMs were fixed, endogenous DDX42 and the nuclei were visualized using DDX42-specific antibodies and Hoechst staining, respectively, and confocal microscopy. Representative images are shown. Scale bar, 10 μm.